



Lawrence Berkeley Laboratory

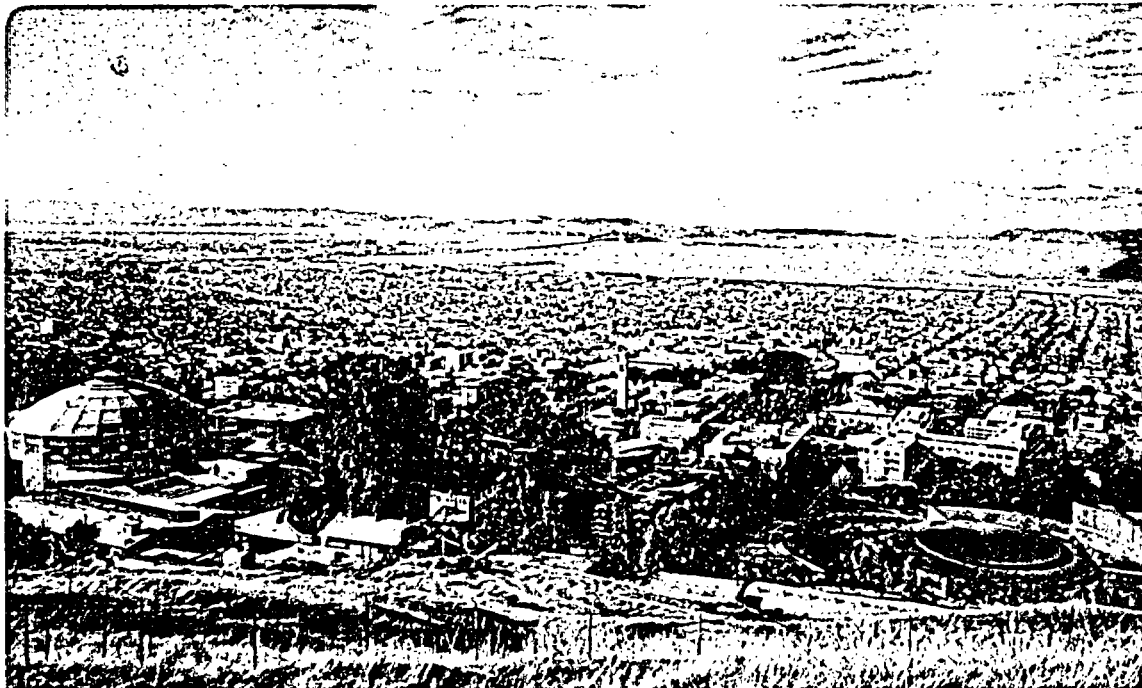
UNIVERSITY OF CALIFORNIA

EARTH SCIENCES DIVISION

HYDROLOGIC MECHANISMS GOVERNING FLUID FLOW IN
PARTIALLY SATURATED, FRACTURED, POROUS TUFF
AT YUCCA MOUNTAIN

J.S.Y. Wang and T.N. Narasimhan

October 1984



HYDROLOGY DOCUMENT NUMBER 227

LEGAL NOTICE

This book was prepared as an account of work sponsored by an agency of the United States Government. Neither the United States Government nor any agency thereof, nor any of their employees, makes any warranty, express or implied, or assumes any legal liability or responsibility for the accuracy, completeness, or usefulness of any information, apparatus, product, or process disclosed, or represents that its use would not infringe privately owned rights. Reference herein to any specific commercial product, process, or service by trade name, trademark, manufacturer, or otherwise, does not necessarily constitute or imply its endorsement, recommendation, or favoring by the United States Government or any agency thereof. The views and opinions of authors expressed herein do not necessarily state or reflect those of the United States Government or any agency thereof.

Printed in the United States of America
Available from
National Technical Information Service
U.S. Department of Commerce
5285 Port Royal Road
Springfield, VA 22161
Price Code: A04

LBL-18473

HYDROLOGIC MECHANISMS GOVERNING FLUID FLOW IN
PARTIALLY SATURATED, FRACTURED, POROUS TUFF
AT YUCCA MOUNTAIN

by

J. S. Y. Wang and T. N. Narasimhan
Earth Sciences Division
Lawrence Berkeley Laboratory
University of California
Berkeley, California 94720

October 1984

ABSTRACT

In contrast to the saturated zone where fluid moves rapidly along fractures, the fractures (with apertures large relative to the size of matrix pores) will desaturate first during drainage process and the bulk of fluid flow would be through interconnected pores in the matrix. Within a partially drained fracture, the presence of a relatively continuous air phase will produce practically an infinite resistance to liquid flow in the direction parallel to the fracture. The residual liquid will be held by capillary force in regions around fracture contact areas where the apertures are small. Normal to the fracture surfaces, the drained portion of the fractures will reduce the effective area for liquid flow from one matrix block to another matrix block. A general statistical theory is constructed for flow along the fracture and for flow between the matrix blocks to the fractures under partially saturated conditions. Results are obtained from an aperture distribution model for fracture saturation, hydraulic conductivity, and effective matrix-fracture flow areas as functions of pressure. Drainage from a fractured tuff column is simulated. The parameters for the simulations are deduced from fracture surface characteristics, spacings and orientations based on core analyses, and from matrix characteristics curve based on laboratory measurements. From the cases simulated for the fractured, porous column with discrete vertical and horizontal fractures and porous matrix blocks explicitly taken into account, it is observed that the highly transient changes from fully saturated conditions to partially saturated conditions are extremely sensitive to the fracture properties. However, the quasi-steady changes of the fluid flow of a partially saturated, fractured, porous system could be approximately simulated without taking the fractures into account.

ACKNOWLEDGEMENTS

We thank S. Sinnock and N. Hayden of Sandia National Laboratories for discussing the tuff data, R. Spengler, R. Scott, and P. Montazer of U. S. Geological Survey for discussing the fracture data. We also thank our colleagues Y. Tsang and K. Pruess for discussing and reviewing the manuscript. This work was supported by the Sandia National Laboratories for the Nevada Nuclear Waste Storage Investigation Project of the U.S. Department of Energy, under contract DE-AC03-76SF00098.

CONTENTS

	<u>Page</u>
Abstract	ii
Acknowledgements	iii
Contents	iv
Figures	v
Glossary	vii
Nomenclature	viii
Introduction	1
Conceptual Model	3
Statistical Theory for Partially Saturated Flow in Rough Fractures	7
Properties of Topopah Spring Member	14
Matrix data	15
Fracture network data	16
Fracture permeability	19
Discrete fracture data	20
Fracture Saturation, Permeability, and Effective Fracture-Matrix Flow Area	21
TRUST Computer Program	27
Fractured Tuff Column Simulations	28
Pressure drop	33
Saturation change	35
Permeability change	37
Effective fracture-matrix flow area change	39
Darcy velocity changes in fractures	39
Darcy velocity changes in fracture-matrix interfaces	42
Summary	44
References	46

FIGURES

<u>No.</u>	<u>Title</u>	<u>Page</u>
1.	Conceptual model of partially saturated, fractured, porous medium showing schematically the flow lines moving around the dry portions of the fractures.	5
2.	Desaturation of fracture surface showing schematically the changes in the fracture plane of liquid phase (shaded areas) configuration from continuous phase at high saturation (top) to discontinuous phase at low saturation (bottom) with liquid forming rings around contact areas (blackened areas). At the cutoff transition (middle), the ratio τ of the liquid flow path W_S to nearest-neighbor air-pocket separation W is zero (see Figure 3 for a unit area around one contact).	10
3.	A unit area around a contact (blackened area) surrounded by liquid (shaded area) and air (clear areas in the corners). The phase-separation constriction factor τ is derived based on geometric calculations.	12
4.	Inclination of fractures in densely welded Topopah Spring Member based on compilation of 1434 fracture data (Spengler and Chornack 1984).	17
5.	Gamma aperture distributions of vertical and horizontal fractures with distribution parameters derived from Topopah Spring Member data.	22
6.	Characteristic curves (saturation vs. head) of vertical fracture, horizontal fracture and tuff matrix with parameters derived from Topopah Spring Member data.	24
7.	Permeabilities of partially saturated discrete fractures and tuff matrix with parameters derived from Topopah Spring Member data.	25
8.	Effective fracture-matrix flow areas at fracture-matrix interfaces with parameters derived from Topopah Spring Member data.	26
9.	Discretization of fractured, porous tuff to represent densely welded Topopah Spring Member.	29
10.	Discretization of one matrix block.	31
11.	Pressure drops.	34
12.	Saturation changes.	36

FIGURES

<u>No.</u>	<u>Title</u>	<u>Page</u>
13.	Permeability changes.	38
14.	Effective fracture-matrix flow area changes.	40
15.	Darcy velocities along discrete fractures (sign convention for horizontal flow: positive - into the intersection, negative - away from the intersection; vertical flow: positive - upward, negative - downward).	41
16.	Darcy velocities at the fracture-matrix interfaces (sign convention for horizontal flow: positive - matrix into fracture, negative - fracture into matrix; vertical flow: positive - upward, negative - downward).	43

GLOSSARY

<u>anisotropic</u>	Having physical properties that vary with direction.
<u>asperity</u>	A type of surface roughness appearing along the fracture surfaces.
<u>bimodal</u>	A distribution with two peaks.
<u>capillary pressure</u>	The difference between the air-phase pressure and the water-phase pressure across a meniscus. If the air-phase pressure is assumed to be atmospheric, capillary pressure is gauge pressure.
<u>Darcy velocity</u>	Bulk velocity of fluid flow as described by Darcy's law, representing an average over the area of the porous medium.
<u>fracture plane inclination</u>	Inclination of the plane of fracture in a rock formation.
<u>isotropic</u>	Having the same properties in all directions.
<u>matrix</u>	The interconnected mass of rock within which water movement is governed by the laws of porous media flow.
<u>pressure head</u>	Pressure expressed as the height of a column of water that can be supported by the pressure.
<u>tortuosity</u>	A parameter in describing the extent to which a fluid-flow departs from a smooth curve along the flow line. Tortuosity results from the diversion of fluid flow around nonconducting volumes in the flow region.

NOMENCLATURE

b	fracture aperture	[L]
b_0	fracture aperture for a fracture under zero stress and with fracture surfaces in point-contact and with zero contact area	[L]
b_c	fracture contact cutoff aperture, portions of fracture with b_0 less than b_c will be in contact	[L]
b_s	saturation cutoff aperture, portions of fracture with aperture greater than b_s will be desaturated	[L]
D	fracture spacing	[L]
f	apparent fracture frequency	[1/L]
f(b)	aperture distribution functions for a fracture under stress, $n(b + b_c)$	[1/L]
g	gravitational acceleration	[L/t ²]
h	pressure head	[L]
h_c	capillary head	[L]
i	hydraulic gradient	
k	continuum saturated permeability	[L ²]
k_r	relative permeability	
$n(b_0)$	aperture distribution function for a fracture under zero stress with fracture surface in point-contact and with zero contact area	[1/L]
Q	volumetric flow rate	[L ³ /t]
S	saturation	
S_r	residual saturation	
W	fracture width	[L]
W_s	width of liquid flow path between dry portions (air pockets) in a fracture	[L]

NOMENCLATURE

α	surface tension	[M/t ²]
β	aperture distribution parameter of gamma distribution	[1/L]
ρ	fluid density	[M/L ³]
σ	fraction of surface area occupied by liquid water and contact areas	
θ	angle of contact between liquid surface and solid surface	
τ	phase separation constriction factor, ratio of width of liquid flow path to the nearest-neighbor dry pocket distance	
μ	fluid viscosity	[M/Lt]
ω	fraction of fracture surface contact area	

Subscript

1	saturated condition $S = 1$
H	horizontal fracture set
S	partially saturated condition at saturation S
V	vertical fracture set
f	fracture
m	porous medium

INTRODUCTION

The work described in this report was performed for Sandia National Laboratories (SNL) as a part of the Nevada Nuclear Waste Storage Investigations (NNSWI) Project. The NNWSI Project is administered by the U.S. Department of Energy's (DOE) Nevada Operations Office. The project is a part of the DOE's program to safely dispose of the radioactive waste from nuclear power plants. DOE has determined that the safest and most feasible method currently known for the disposal of such wastes is to emplace them in mined geologic repositories. The NNWSI project is evaluating the suitability of Yucca Mountain on and adjacent to the Nevada Test Site (NTS) in southern Nevada to determine the feasibility of developing a repository for high level nuclear wastes.

The objective of this report is to aid the performance assessment activities in the NNWSI Project by addressing the hydrologic mechanisms governing fluid flow in partially saturated, fractured, porous tuff at Yucca Mountain. The focus of this report is on the understanding how fractures and porous matrix affect the transient and steady-state fluid flow behavior. The goal is to determine whether a partially saturated, fractured, porous tuff can be idealized as an equivalent continuum combining properties of the fractures and matrix, or as a system of multiple continua in which the fractures, matrix and their interactions are modeled.

One of the candidate horizons for a nuclear waste repository at Yucca Mountain is the densely welded, devitrified, nonlithophysal zone of the Topopah Spring Member above the water table. Densely welded ash-flow tuffs generally have low matrix hydraulic conductivities but tend to contain

numerous fractures that may be highly transmissive (Sinnock et al., 1984). Fractures may be important either as conduits or as barriers for flow of groundwater. In the saturated zone, water tends to move rapidly along fractures. However, for a fractured unit above the water table, the fractures (whose apertures are large relative to the size of the pores in the matrix) should be dry and the bulk of the groundwater movement should be through interconnected pores in the matrix. Under this condition, as water moves from one matrix block to another, the drained portions of the fractures will reduce the effective area for water flow from one matrix block to another matrix block.

In this report, we will (1) describe a conceptual model for the hydrology of a partially saturated, fractured, porous medium; (2) construct a general statistical theory for flow along the fractures and for flow between the matrix blocks and the fractures under partially saturated conditions; (3) present the results obtained from a simple statistical aperture distribution model for fracture saturation, hydraulic conductivity, and effective matrix-fracture flow area as functions of pressure; (4) review the available data for the fractured Topopah Spring Member and the needs for additional data to improve and validate the statistical theory; (5) summarize the recent updates of the numerical code TRUST for handling partially saturated, fractured, porous flow systems; and (6) present the results of simulations of a fractured tuff column in response to drainage.

CONCEPTUAL MODEL

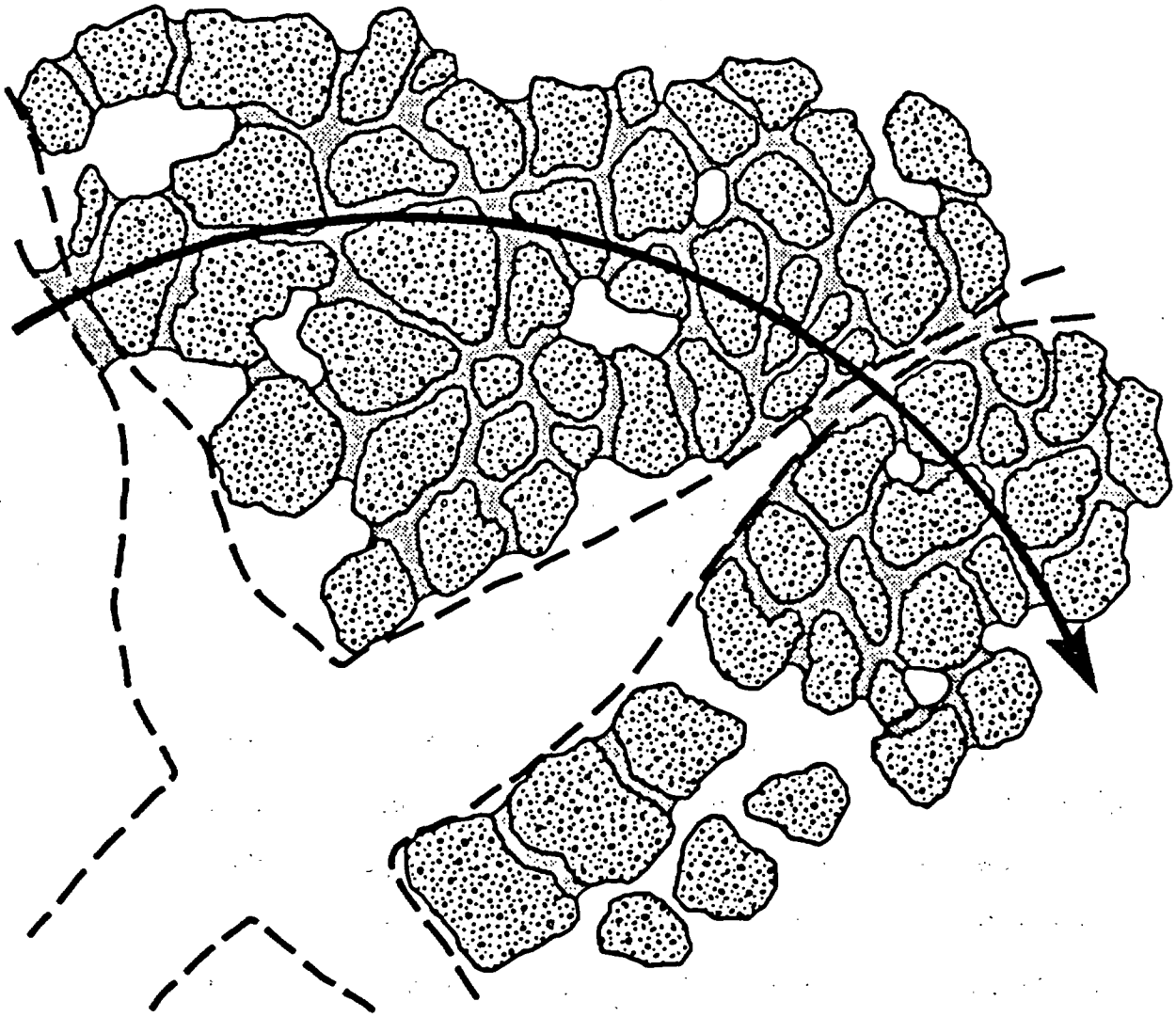
To study the flow of water in a partially saturated fractured porous medium, we first formulate a conceptual model based on the basic principles of soil physics. Tuff is a consolidated rock made up essentially of cemented volcanic ash. The primary pore size of the tuff at Yucca Mountain ranges from a few to a few tens of microns (Blair et al., 1984). Even at a depth of several hundred meters in such a formation, the fractures are likely to have apertures ranging from several tens to several hundreds of microns. Thus fractured tuff will have a strongly bimodal pore size distribution. It is well established in the field of soil physics that in partially saturated porous media, the fluid pressure in the water phase is less than atmospheric pressure and that the fluid saturation in the porous medium is a strong function of the water phase pressure. The relation between fluid pressure and saturation is governed by surface tension between the liquid and the solid phases and by the effective capillary radii of the pores. Indeed, it is accepted knowledge that as the water phase pressure in the porous medium is decreased below atmospheric pressure, the largest pores will desaturate first, followed by the desaturation of successively smaller pores.

If one recognizes that the large pores desaturate first during the drainage process, it is easy to infer that the fractures in a fractured porous medium will tend to remain dry under conditions of partial saturation and that water will be held by capillarity in the finer pores of the matrix. Moreover, because natural fractures are characterized by rough surfaces, the aperture of a fracture is seldom spatially constant and will be very small near asperities. Thus one would expect that asperities will cause "islands" of water film to be held within the fracture plane. Within a fracture that

is partially saturated in this fashion, the presence of a relatively continuous air phase will produce an almost infinite resistance to liquid flow in a direction parallel to the fracture. Therefore, as a fracture begins to desaturate, its effective hydraulic conductivity will decline abruptly by several to many orders of magnitude. It is reasonable to expect that during fracture desaturation the effective hydraulic conductivity of the fractures will rapidly become smaller than that of the porous matrix, which needs fairly large capillary pressures to initiate desaturation.

An interesting consequence of this dramatic reduction in fracture permeability is that water will tend to flow across fractures from one matrix block to another instead of flowing along the fractures. Thus, one may expect flow lines to circumvent dry portions of the fractures (Figure 1). The fractures will thus introduce a macroscopic tortuosity in the system. If this reasoning is sound, one may grossly quantify the effects of the fractures in terms of an overall tortuosity factor, a task that may prove to be somewhat simpler than characterizing a saturated fractured system as an equivalent anisotropic medium.

In order to quantitatively evaluate the hydrology of a fractured porous medium, three basic relations are required: (1) the relation between fluid pressure head (which is less than atmospheric under partial saturation) and fracture saturation, (2) the relation between fluid pressure head and fracture conductivity, and (3) the proportion of the fracture surface that remains wetted. To date, no data are experimentally available for these relations for the Yucca Mountain rocks. In order to gain insight into the problem, it is necessary to develop these relations on theoretical grounds using fracture roughness characteristics and surface tension characteristics.



XBL 841-9580

Figure 1. Conceptual model of partially saturated, fractured, porous medium showing schematically the flow lines moving around the dry portions of the fractures.

The capillary theory and flow law for rough fractures are the building blocks with which we construct our development of theoretical formulae for fracture saturation, hydraulic conductivity, and effective fracture surface area.

Capillary pressure determines the water-phase pressure at which a given size fracture or pore will drain. From force balance, the height of rise for an idealized parallel-plate, smooth-wall fracture with aperture b is

$$h_c = -h = \frac{2\alpha \cos\theta}{b\rho g} \quad (1)$$

With the gravitational acceleration g , water density ρ , surface tension α , and the angle of contact θ between liquid surface and solid surface remaining constant at ambient temperature, the capillary head h_c or the pressure head h is inversely proportional to the aperture b . We use $\theta = 0^\circ$, $\alpha = 0.07183 \text{ kg/sec}^2$, $\rho = 1000 \text{ kg/m}^3$, and $g = 9.80665 \text{ m/sec}^2$ in our calculations. Using the capillary theory for a set of parallel, smooth-wall fractures at given negative pressure head, h , fractures with apertures larger than that determined by Equation 1 will be drained (Evans and Huang, 1982).

If the capillary theory is applied to a real fracture with rough wall and variable aperture, this equation indicates that the sections of large aperture will drain first as the magnitude of the capillary suction increases (or the pressure head becomes more negative). Two important phenomena will occur as the fracture desaturates: (1) along the fracture surface, air pockets will form and impede the flow, thereby reducing its effective permeability for liquid flow, (2) normal to the fracture surface, the flow between adjacent matrix blocks across the fractures will occur only through the sections of the fracture that remain saturated. Unsaturated portions within the fractures will then become barriers to liquid flow both along the fractures and normal to the fractures between the adjacent matrix blocks.

In this simple conceptualization, we ignore film flow on partially saturated rock surfaces, vapor transport from evaporation-condensation across the liquid phases, drying processes of isolated liquid pockets surrounded by gaseous phases, and solubility of air in water. It is possible to extend the quantitative statistical theory to be presented in the next section to include these phenomena. However, for simplicity, we will ignore these mechanisms and focus on the consequences induced by the desaturation of fractures on the liquid fluid flow through partially saturated, fractured, porous tuff.

STATISTICAL THEORY FOR PARTIALLY SATURATED FLOW IN ROUGH FRACTURES

The scale of primary interest in our study is of the order of the size of matrix blocks separated by discrete fractures. The much smaller scale around individual fracture asperities is not of practical interest for fluid flow assessment modeling, and a statistical averaging procedure, applied over this smaller scale, is assumed to be sufficient to take into account the controlling mechanisms governing the desaturation of sections of larger apertures and the resultant reduction in fracture and matrix flows.

The statistical description of a rough-wall, variable-aperture fracture begins with the aperture distribution function $n(b_0)$ for a fracture under zero stress (Tsang and Witherspoon, 1981). Under zero stress, the fracture surfaces are in point contact with zero contact area between the walls and all spaces between the fracture surfaces can transmit fluid. The aperture distribution function $n(b_0)$ can be measured by scanning the open fracture surfaces and tracing the roughness profiles. The mismatch between the roughness profiles between the two surfaces yields the aperture distribution function $n(b_0)$ (Tsang, 1984).

For in situ fractures, the stress is greater than zero and the fracture surfaces will be in contact. The fraction of contact area, ω , of the total area of the fracture at any stress can be expressed as

$$\omega = \int_0^{b_c} n(b_0) db_0 \quad (2)$$

The averaging over aperture is equivalent to normalized areal integration over fracture surface plane. All the portions of fracture with initial aperture less than the contact cutoff aperture b_c will be in contact. The aperture under stress will be $b = b_0 - b_c$ in the open sections of the fracture. The aperture distribution of the fracture under stress will be denoted by $f(b)$, which is

$$f(b) = n(b + b_c) \quad (3)$$

For fully saturated flow of water in the fractures, the cubic law, derived from the solution (Boussinesq, 1868) of an idealized parallel plate representation of the fracture, is valid from experimental studies on a set of artificially induced tension fractures of hardrock samples (Witherspoon et al., 1980). For laminar flow through a fracture with lateral width W and with uniform aperture b , the volumetric flow rate Q is

$$Q = W \cdot \frac{\rho g}{\mu} \cdot \frac{b^3}{12} \cdot i \quad (4)$$

where i is the hydraulic gradient and μ is the fluid viscosity. For a fracture with variable aperture, one may generalize the cubic law by replacing the cube of the single value for the aperture by an average $\langle b^3 \rangle$

$$\langle b^3 \rangle_1 = \int_{b_{\min}}^{b_{\max}} b^3 f(b) db \quad (5)$$

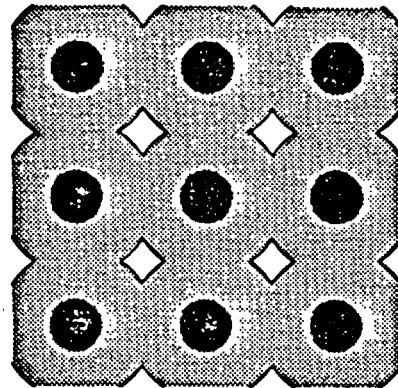
If this generalization of the cubic law is assumed valid, then this average determines the saturated conductivity of a variable-aperture fracture. The subscript 1 denotes the saturated condition $S = 1$.

The basic assumption in using $\langle b^3 \rangle$ is that all the flow paths within a fracture are parallel to the direction of flow (Tsang and Witherspoon, 1981). The tortuosity of flow paths, introduced by the presence of contact area forcing the fluid to circulate around it, is not taken into account. For fractures with a small percentage of contact area, the generalized cubic law may be a good formula to describe the flow through a variable-aperture fracture. Recent numerical experiments with random flow path network simulations show that the generalized cubic law overestimates the fracture conductivity for fractures with high percentage of contact area (Tsang, 1984). The tortuosity of flow paths within a rough fracture becomes an important factor in determining fracture conductivity and additional resistance due to the presence of large contact area must be taken into account. In this study, we assume that in the portions of the fractures away from the immediate vicinity of contact areas, the average flow through the open channels can still be described by $\langle b^3 \rangle_1$.

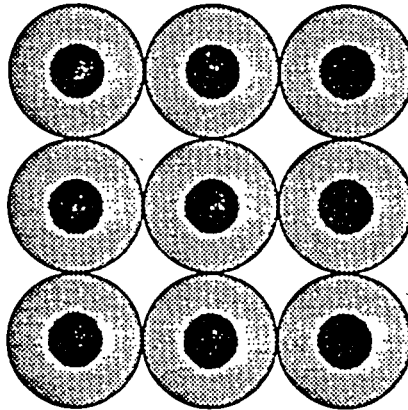
As the fracture desaturates under a negative pressure head, h , the portions of the fractures with aperture greater than the saturation cutoff aperture b_S ,

$$b_S = - \frac{2\alpha \cos\theta}{\rho g h} , \quad (6)$$

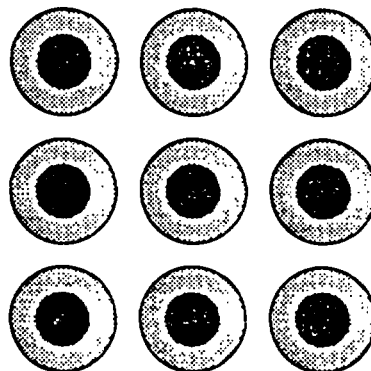
will be desaturated and unable to transmit liquid flow. The portions with large apertures are likely to be located away from the contact areas, with the water remaining around the contact areas. Figure 2 shows schematically the changes of liquid phase configuration on a fracture surface plane during the



$0 < \tau < 1$
Continuous
liquid phase



$\tau = 0$
Cut off



$\tau = 0$
Discontinuous
liquid phase

XBL 842-9615

Figure 2. Desaturation of fracture surface showing schematically the changes in the fracture plane of liquid phase (shaded areas) configuration from continuous phase at high saturation (top) to discontinuous phase at low saturation (bottom) with liquid forming rings around contact areas (blackened areas). At the cutoff transition (middle), the ratio τ of the liquid flow path W_s to nearest-neighbor air-pocket separation W is zero (see Figure 3 for a unit area around one contact).

desaturation process. If the liquid phase is continuous (Figure 2, top), the liquid can flow along the fracture plane with effective width of flow determined by the width of the neck (W_S in Figure 2) between nearest-neighbor dry areas (air pockets). The ratio of neck width, W_S , to the nearest-neighbor distance, W , can be quantified as an effective phase-separation constriction factor to take into account the blockage of flow by the air pockets and the change of flow paths in swinging around these dry areas.

For the particular geometry shown in Figure 2, the phase-separation constriction factor $\tau = W_S/W$ can be determined by the root of the equation

$$\tau + (1 + \tau^2) \left(\frac{\pi}{4} - \tan^{-1}(\tau) \right) = \sigma \quad (7)$$

where σ is the effective fraction of area occupied by the liquid water and contact areas (see Figure 3 for the deviation of this formula). If σ is less than $\pi/4$, the liquid phase is discontinuous on the fracture surface and liquid cannot flow along the fracture (Figure 2, bottom). Therefore, $\sigma = \pi/4$ or $\tau = 0$ determines the cutoff for fracture flow for a partially saturated fracture (Figure 2, middle).

Within the liquid phase away from the immediate vicinity of contact areas, the effective average cube aperture is

$$\langle b^3 \rangle_S = \int_{b_{\min}}^{b_S} b^3 f(b) db \quad (8)$$

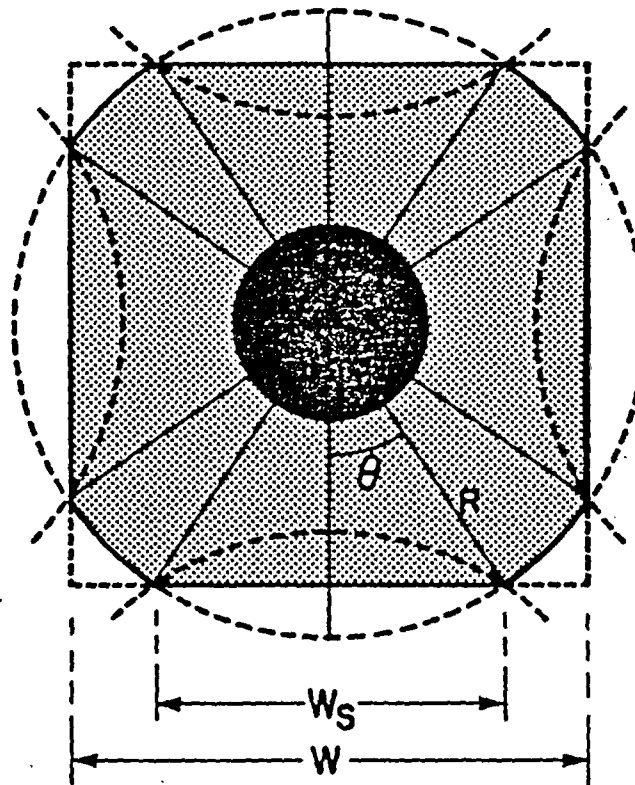
The relative permeability for the fracture, defined as the ratio of conductivity at saturation S to that at saturated condition $S = 1$, is therefore

$$\tan \theta = \frac{W_s}{W} = \tau$$

$$R = \left(\frac{W_s}{2}\right)^2 + \left(\frac{W}{2}\right)^2$$

$$4 \times \frac{1}{2} (W_s \times \frac{W}{2}) + \pi R^2 \left(\frac{2\pi - 8\theta}{2\pi}\right) = W^2 \sigma$$

$$\tau + (1 + \tau^2) \left(\frac{\pi}{4} - \tan^{-1} \tau\right) = \sigma$$



XBL 842-9612

Figure 3. A unit area around a contact (blackened area) surrounded by liquid (shaded area) and air (clear areas in the corners). The phase-separation constriction factor τ is derived based on geometric calculations.

$$k_r(h) = \tau \frac{\langle b^3 \rangle_S}{\langle b^3 \rangle_1} \quad (9)$$

The saturation of the fracture is determined by the fraction of fracture opening occupied by the liquid water. Since the averaging over apertures is equivalent to areal integration over fracture surface planes, and fracture volume is the product of aperture and area, we have

$$S(h) = \frac{\langle b \rangle_S}{\langle b \rangle_1} \quad (10)$$

Flow from the matrix into the fracture and through the fracture into the next matrix block can occur only in the saturated sections and in the contact areas. Since sections with apertures less than the saturation cutoff aperture b_S will be saturated, the effective fraction of area for fracture-matrix flow is

$$\sigma(h) = \omega + \int_{b_{\min}}^{b_S} f(b) db \quad (11)$$

Equations 9, 10 and 11 can be used to determine k_r , S , and σ for any given aperture distribution. No data are available for tuff to determine the aperture distribution functions $n(b_0)$ or $f(b)$. Recent analysis of natural granite fractures shows that $n(b_0)$ takes on a skewed shape, with long tails toward large apertures (Tsang, 1984). A one-parameter distribution, the gamma distribution, could fit the aperture measurements well. The gamma distribution is simply

$$n(b_0) = \beta^2 b_0 e^{-\beta b_0} \quad (12)$$

With this simple functional form, analytic expressions for the fracture relative permeability, k_r , saturation, S , and effective fracture-matrix flow area, σ , can be derived:

$$\langle b^3 \rangle_1 = \frac{6(4 + \beta b_c)}{\beta^3} \exp(-\beta b_c) \quad (13)$$

$$k_r(h) = \tau \frac{1}{6(4 + \beta b_c)} \left\{ \left[24 - \exp(-\beta b_S) (24 + 24\beta b_S + 12\beta^2 b_S^2 + 4\beta^3 b_S^3 + \beta^4 b_S^4) \right] + \beta b_c \left[6 - \exp(\beta b_S) (6 + 6\beta b_S + 3\beta^2 b_S^2 + \beta^3 b_S^3) \right] \right\} \quad (14)$$

$$S(h) = \frac{1}{1 + 2\beta b_c} \left\{ \left[2 - \exp(-\beta b_S) (2 + 2\beta b_S + \beta^2 b_S^2) \right] + \beta b_c \left[1 - \exp(-\beta b_S) (1 + \beta b_S) \right] \right\} \quad (15)$$

$$\sigma(h) = 1 - \exp(-\beta b_c - \beta b_S) (1 + \beta b_c + \beta b_S). \quad (16)$$

where the contact cutoff aperture, b_c , is determined by the root of the equation

$$1 - \exp(-\beta b_c) (1 + \beta b_c) = \omega. \quad (17)$$

The parameters β and b_c are determined from available tuff properties discussed in the next section.

PROPERTIES OF THE TOPAPAH SPRING MEMBER

To model fluid flow through partially saturated, fractured, porous tuff of the Topopah Spring Member, we need data on discrete fractures, fracture network, and matrix properties. The data used in this analysis are based on the data

provided by SNL (Hayden, et al., 1983), supplemented by data in the literature. For those properties needed for the simulation but not yet available, the formulae presented in this report are used. All parameters in the formulae are determined by the data. The formulation and statistical theory in this report can accommodate detailed fracture and matrix data, and no adjustable parameter needs to be introduced in the simulations.

Matrix Data

The data are mainly from laboratory measurements of core samples from different boreholes at Yucca Mountain:

- o matrix saturated permeability $3.263 \times 10^{-17} \text{ m}^2$ or $3.2 \times 10^{-8} \text{ cm/sec}$ from borehole USW-GU3,
- o matrix saturation 0.8 or 80%, from boreholes USW-GU3 and USW-G4,
- o matrix characteristic curve

$$S = (1 - S_r) \left[\frac{1}{1 + |Ah|B} \right]^{(1 - \frac{1}{B})} + S_r, \text{ and} \quad (18)$$

- o matrix relative permeability

$$\frac{k_m(S)}{k_m(1)} = [1 + |Ah|B]^{-\lambda/2} \left\{ 1 - \left[\frac{|Ah|B}{1 + |Ah|B} \right]^\lambda \right\}^2 \quad (19)$$

where $S_r = 9.6 \times 10^{-4}$

$$A = 7.027 \times 10^{-3} \text{ 1/m}$$

$$B = 1/0.45 = 1.818$$

$$\lambda = 1 - 1/B = 0.55$$

These values were obtained by a least square fit (Peters and Gauthier, 1984) to the empirical data from borehole USW-GU3 with the equation used by van Genuchten (1980). In our simulations, the matrix saturation will vary between the fully saturated condition, $S = 1$, and the in situ matrix saturation, $S = 0.8$, a range far away from the residual saturation, S_r , which usually is poorly measured and poorly fitted. The relative permeability formula is derived from the characteristic curve formula by van Genuchten (1980) following the theory of Mualem (1976).

Fracture Network Data

Fracture patterns, orientations, and spacings have been measured in borehole cores and from surface mapping. The fracture data of the Topopah Spring Member (Spengler and Chornack, 1984) from borehole USW-G4 include:

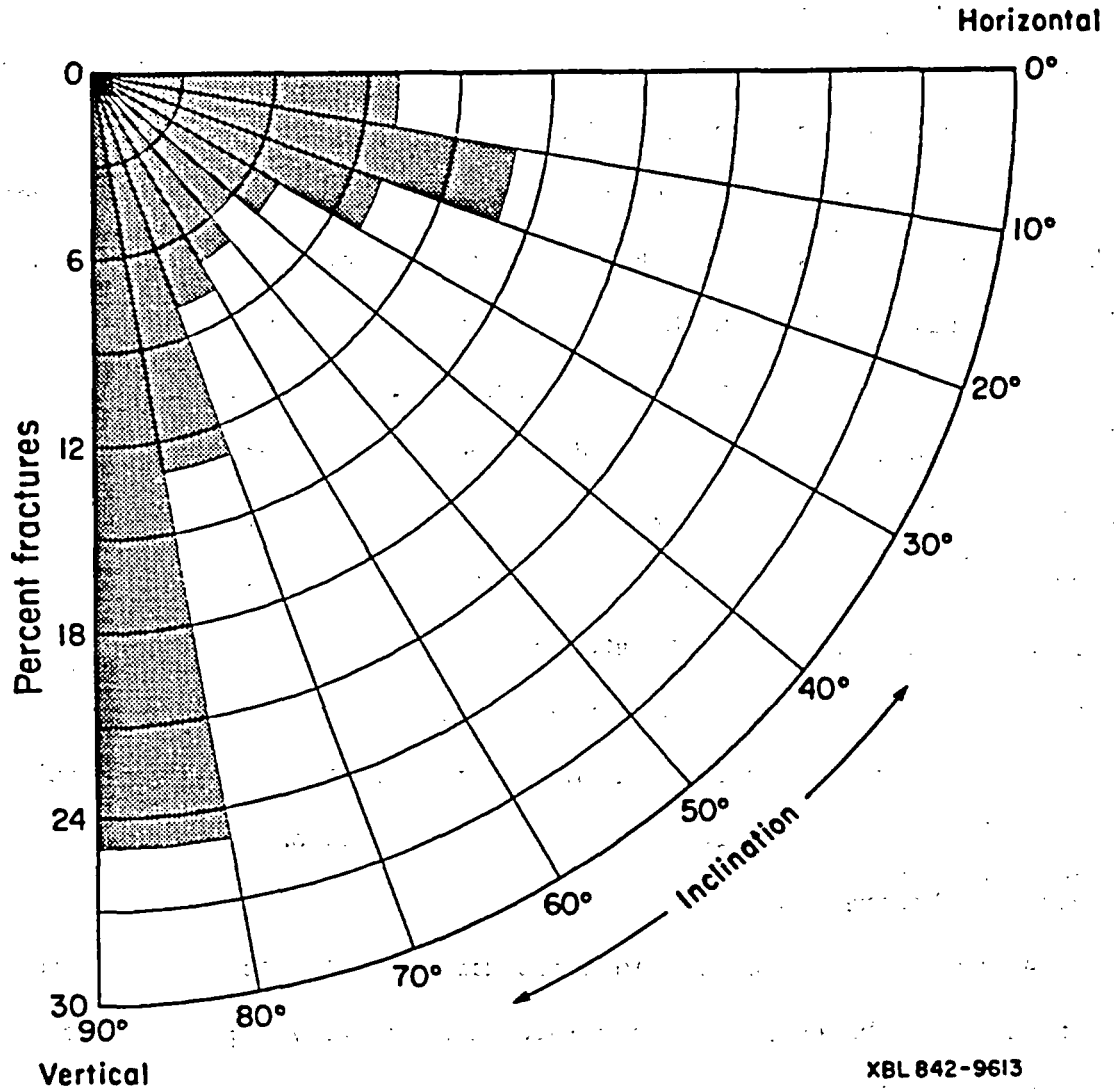
- o apparent fracture frequency, $f = 4.36/m$, and
- o distribution of fracture inclination (dipping angle between 0° and 90°) as shown in Figure 4.

Figure 4 shows that the fracture inclinations in densely welded Topopah Spring Member may be grouped into two categories. 56% of the fractures have steep dipping inclinations ($>45^\circ$) and can be classified as nearly vertical fractures. 44% of the fractures have low dipping inclinations ($<45^\circ$) and may be classified as nearly horizontal. The averages of the cosine of the dip angles for each group in the distribution of Figure 4 are:

$$\langle \text{COS} \rangle_V = 0.2689 \quad (20)$$

$$\langle \text{COS} \rangle_H = 0.9183 \quad (21)$$

The subscripts V and H represent the nearly vertical and nearly horizontal group, respectively. These cosine averages, together with the overall



XBL 842-9613

Figure 4. Inclination of fractures in densely welded Topopah Spring Member based on compilation of 1434 fracture data (Spengler and Chornack 1984).

apparent fracture spacing of $f = 4.36/\text{m}$ in borehole USW-G4, are used to determine the spacings of the nearly vertical and nearly horizontal fracture sets:

$$D_V = \frac{\langle \text{COS} \rangle_V}{f} = 0.2203 \text{ m} \quad (22)$$

$$D_H = \frac{\langle \text{COS} \rangle_H}{f} = 0.4786 \text{ m} \quad (23)$$

These spacings are used in the simulations to determine the dimensions and size of the matrix blocks partitioned by the fractures.

From surface mapping, there are two nearly vertical fracture sets dipping steeply ($60^\circ - 90^\circ$), one strikes north-northwest, one strikes north-northeast (Scott et al., 1982). The NNW set has higher density but may tend to have smaller apertures than those with NNE trends. The regional stress field is oriented with the maximum horizontal compressive stress in the NE direction (Carr, 1974). Data are not available to distinguish between the hydraulic properties of the two sets. We assume that the contributions from each set to the equivalent continuum saturated conductivity (cube of aperture divided by spacing) are equal. We also assume that equivalent fracture continuum conductivity is isotropic. All these simplifying assumptions about the fracture network can be relaxed easily when additional and more detailed field data become available.

Along a given direction in three dimensional space, two fracture sets contribute to the equivalent continuum conductivity, k_f . We have

$$\frac{k_f}{2} = \frac{\langle b^3 \rangle}{12D} \quad (24)$$

for each set with spacing D .

The interconnection of fractures in the welded tuff is demonstrated by hydrologic tests near Yucca Mountain, which shows that the volume of water removed during pumping tests is much greater than the volume of the fractures close to the drill holes (Thordarson, 1983). The several orders of magnitude difference between the laboratory measurements of matrix permeability and the field measurements of in situ permeability, discussed in the next paragraph, supports the assumption that fractures form a continuous, connected network that provides an effective pathway for fluid movement under saturated conditions.

Fracture Permeability

The data base for fracture permeability is taken from results of a Performance Assessment Working Group (PAWG) meeting held in San Francisco on 06/23-24/83 (Tyler, 1983):

- o fracture continuum saturated permeability $k_f = 1.0197 \times 10^{-11} \text{ m}^2$
or 10^{-2} cm/sec (range $10^{-2} - 10^{-4} \text{ cm/sec}$) :

This fracture saturated conductivity is deduced from well testing in well J-13 and is assumed to represent the equivalent fracture continuum (S. Sinnock, SNL, personal communication, 10/10/83; Thordarson, 1983). Well J-13 is located in a low-standing structural block with part of the Topopah Spring Member saturated. The high in situ conductivity of the Topopah Spring Member in Well J-13 may be caused in part by the presence of faults and associated fractures. In the NTS, highly fractured, densely welded tuffs have effective hydraulic conductivities that are approximately 5 or 6 orders of magnitude larger than the matrix hydraulic conductivities (Winograd and Thordarson, 1975). However, knowledge of hydrologic properties of

unsaturated unit at Yucca Mountain is incomplete. Preliminary analysis of air permeability tests on borehole UE25A-4 indicates that the densely welded Topopah Spring Member may be more conductive than the values quoted by Winograd and Thordarson (1975) (P. Montazer, USGS, personal communication in Environmental Assessment Planning Meeting, 10/25/83). We tentatively chose 10^{-2} cm/sec as the saturated value of hydraulic conductivity k_f of the fracture continuum. This parameter is one of the most important hydrologic data in determining the flow field at Yucca Mountain.

Discrete Fracture Data

The data for fracture surface roughness and aperture distributions are being measured, but not yet available. We used an indirect data from borehole USW-G4 core analysis (Spengler and Chornack, 1984) that indicates:

- o Fracture coatings $\omega = 12\%$ with zeolites, clay, calcite.

The fracture coatings of 12% are assumed to correspond to the fraction of in situ contact area. The identification of fracture coating with contact area is a novel assumption. Further study will examine the credibility of this identification. The contact area can also be determined independently with flow-stress-fracture displacement measurements. For granite and basalt, the fractional contact areas at 20 MPa normal stress are in the range of 15 - 20%. (Tsang and Witherspoon, 1981; Iwai, 1976). The fractional contact area of 12% for tuff, based on the assumption that hydrochemical alterations occur in contact areas which remain at continuous contact with water for a long time, may be a reasonable estimate.

FRACTURE SATURATION, PERMEABILITY AND EFFECTIVE FRACTURE-MATRIX FLOW AREA

With the available data and explicit formulae derived for the gamma aperture distribution, the partially saturated fracture properties as functions of negative pressure head can be calculated and used in the TRUST program. In summary, the calculational steps are:

- (1) With $\omega = 12\%$, βb_c is determined by Eq. 17.
- (2) With $k_f = 1.0197 \times 10^{-11} \text{ m}^2 = 10^{-2} \text{ cm/sec}$, and spacing D_V, D_H of Eqs. 22, 23, the β 's are determined by:

$$\beta^3 = \frac{(4 + \beta b_c) \exp(-\beta b_c)}{D k_f} \quad (25)$$

The results are

$$\beta_V = 1.041 \times 10^4 \text{ 1/m} \quad (26)$$

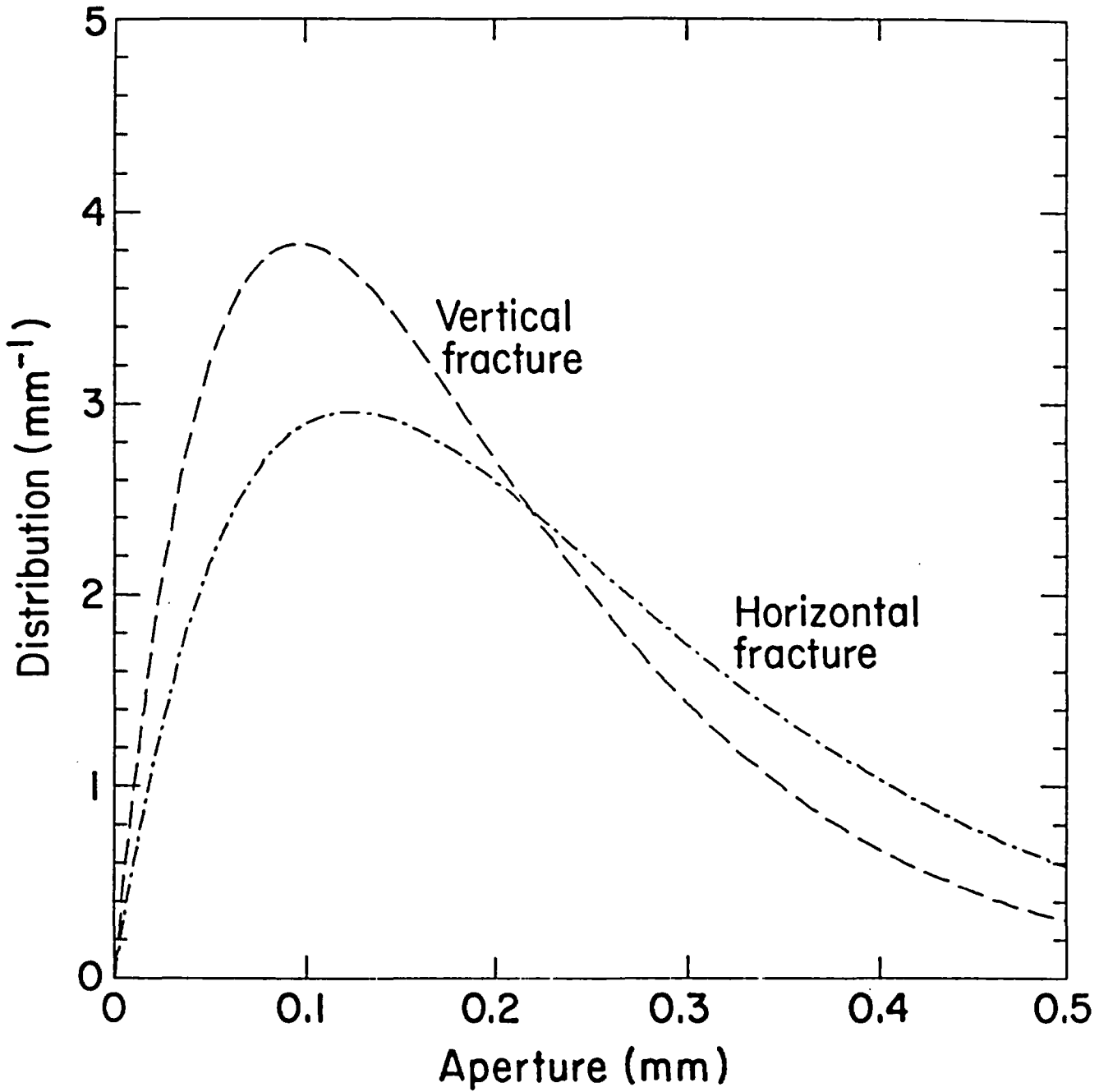
$$\beta_H = 0.8039 \times 10^4 \text{ 1/m} \quad (27)$$

The aperture distribution functions with these distribution parameters are plotted in Figure 5. The contact cutoff aperture, b_c , is derived to be 0.05707 mm for the vertical fractures and 0.07391 mm for the horizontal fractures. The average apertures, defined as the cubic root of the cube average, $[\langle b^3 \rangle_1]^{1/3}$, are

$$\bar{b}_V = 0.2380 \text{ mm} \quad (28)$$

$$\bar{b}_H = 0.3082 \text{ mm} \quad (29)$$

- (3) With b_s given by Eq. 6, and the formulae of Eqs. 14, 15 and 16, the fracture saturation, discrete fracture permeability, $k_r \bar{b}^2/12$, and effective fracture-matrix flow area can be calculated as functions of negative pressure head. These relationships are plotted in Figures 6, 7, and 8. The matrix saturation of Eq. 18 and permeability of Eq. 19 are also plotted for comparison.



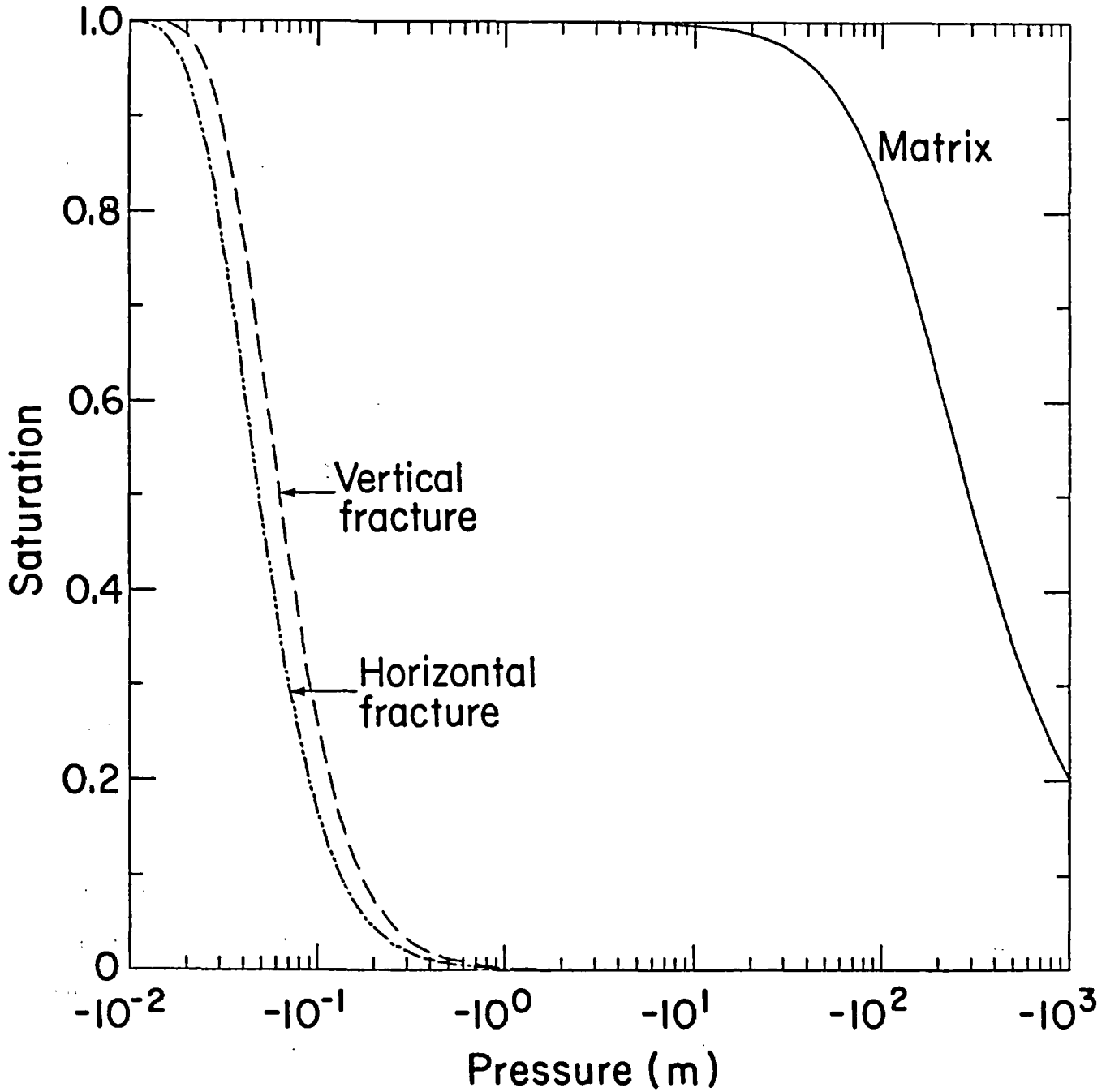
XBL842-9616

Figure 5. Gamma aperture distributions of vertical and horizontal fractures with distribution parameters derived from Topopah Spring Member data.

Figure 6 shows that fractures can desaturate easily with a small suction of -10^{-1} m. The saturation in the matrix will remain high. If the in situ matrix saturation is 0.8, then the negative pressure head in Topopah Spring Member is -111.6 m. With such a large suction, the fracture saturations will be essentially zero.

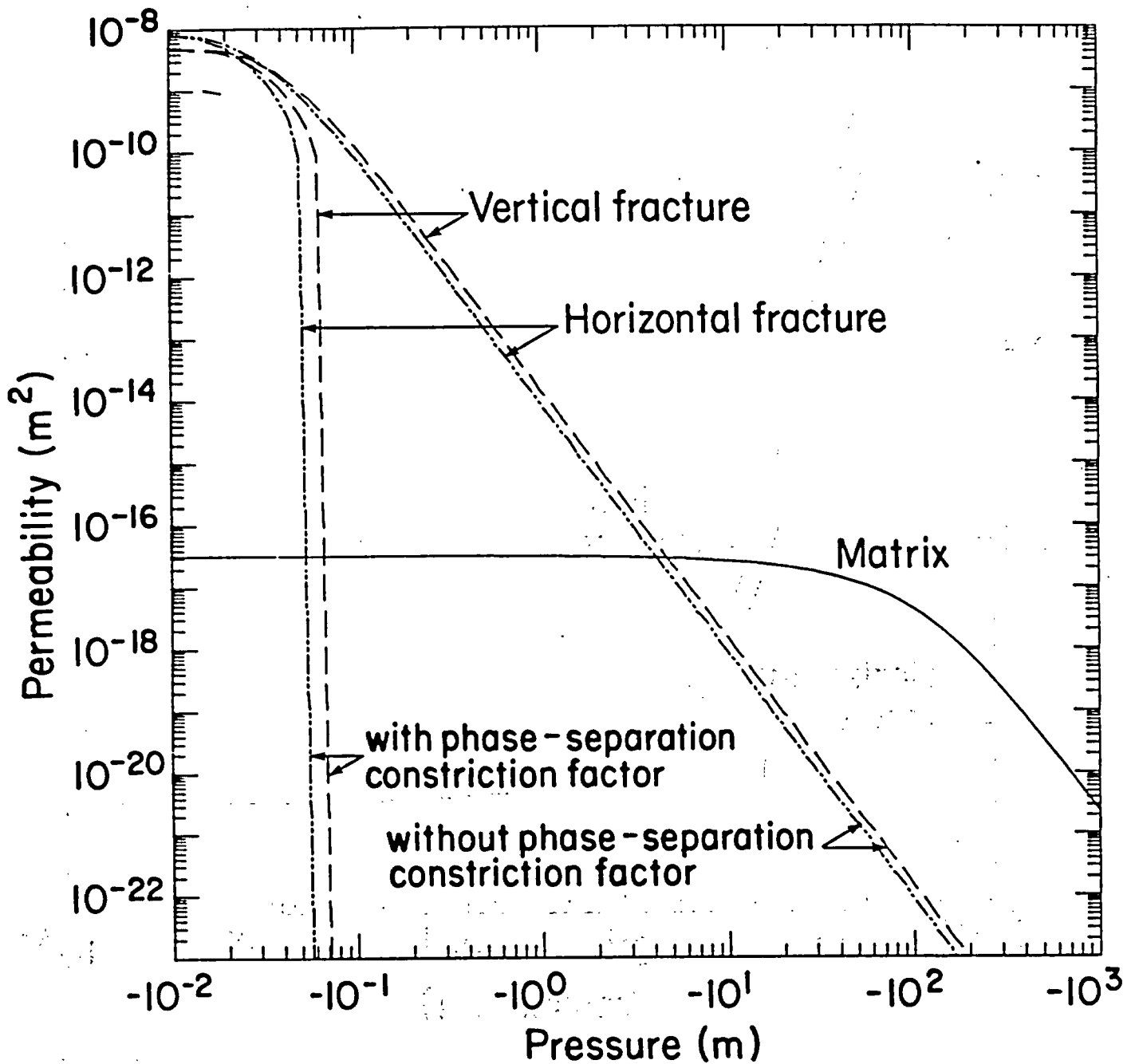
Figure 7 shows that the fracture permeabilities are very sensitive to suction. If fully saturated, the permeability of each discrete fracture is 8 orders of magnitude greater than the matrix permeability. The equivalent fracture continuum permeability is 3.1×10^5 greater than the matrix permeability. With small suctions in the range -10^{-1} to -10^1 m, the discrete fracture permeabilities decrease drastically. The matrix permeability decreases much more gently as the pressure head becomes more negative. Near fully saturated conditions, the fractures will control the fluid flow. As desaturation proceeds and the fracture permeability of each discrete fracture become less than the matrix permeability, the matrix will control the flow. For in situ suction of -111.6 m in the Topopah Spring Member, fracture flow is negligible and matrix flow dominates.

Two sets of discrete fracture permeabilities are plotted in Figure 7, one with the phase-separation constriction factor τ of Eq. 7 taken into account, one with $\tau = 1$. The phase-separation constriction factor takes into account the effects of blockage of flow by air pockets, the flow-path distortion around the air pockets and the presence of a discontinuous liquid phase with fluid remaining stationary around fracture surface contacts. The cases with $\tau = 1$ ignore the blockage effects and take into account only the generalized cubic law for fracture flow. With $\tau = 1$, we overestimate the fracture



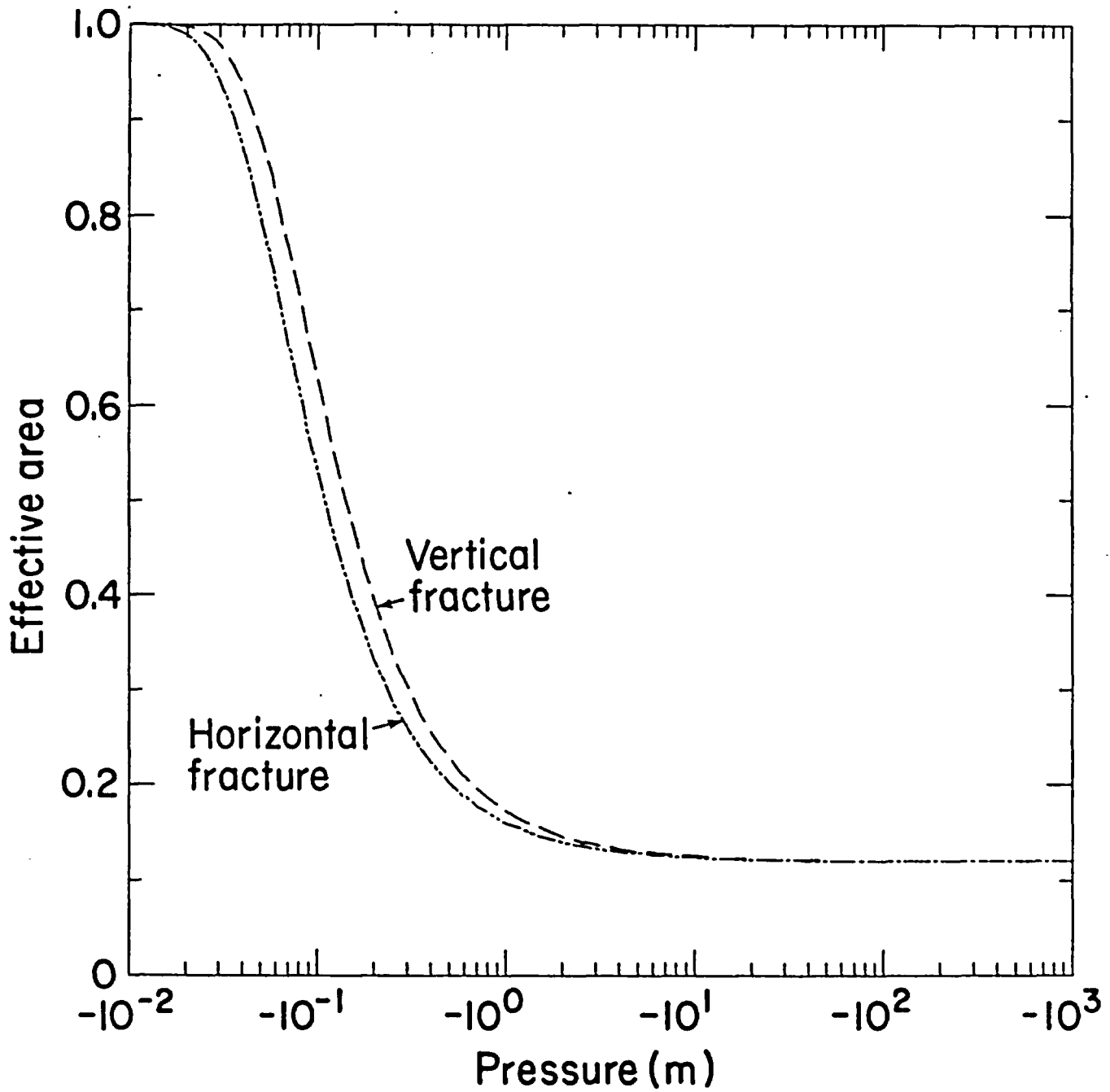
XBL 842-9617

Figure 6. Characteristic curves (saturation vs. head) of vertical fracture, horizontal fracture and tuff matrix with parameters derived from Topopah Spring Member data.



XBL842-9620

Figure 7. Permeabilities of partially saturated discrete fractures and tuff matrix with parameters derived from Topopah Spring Member data.



XBL 842-9621

Figure 8. Effective fracture-matrix flow areas at fracture-matrix interfaces with parameters derived from Topopah Spring Member data.

permeabilities and ignore the zero fracture permeability cutoff. The effects of this phase-separation constriction factor will be discussed in the simulation results.

The matrix flow also will be impeded when it crosses the fractures. The matrix-fracture flow is limited by the available area in the fracture surfaces for fluid to transmit through. Figure 8 shows that the effective fracture-matrix flow area decreases and quickly approaches the limiting contact area fraction, ω , as the pressure head decreases. The effective fracture-matrix flow area reduces the available area for matrix flow across the matrix-fracture interfaces. With liquid flow from one matrix block to another restricted to cross the interfaces through reduced areas, the flow lines will bunch around asperities and flow paths will be more tortuous in a partially saturated, fractured porous medium.

TRUST COMPUTER PROGRAM

To implement the conceptual model and statistical formulation, the computer code TRUST (Narasimhan et al., 1978) has been updated in several respects. Additional characteristic curves and relative permeability curves were programmed. The van Genuchten (1980) formulae are needed to simulate the matrix blocks. The gamma distribution formulae will be used for the discrete fracture grid blocks. Also included are the hyperbolic characteristic curves used by Pickens et al. (1979).

The areas between neighboring nodes are multiplied by a new effective area factor to account for the changes of flow areas in fracture-matrix connections. Two options are programmed for the effective area factor: the gamma distribution effective area formula or any tabulated data. If experimental data on fracture aperture distributions are available, it may be more

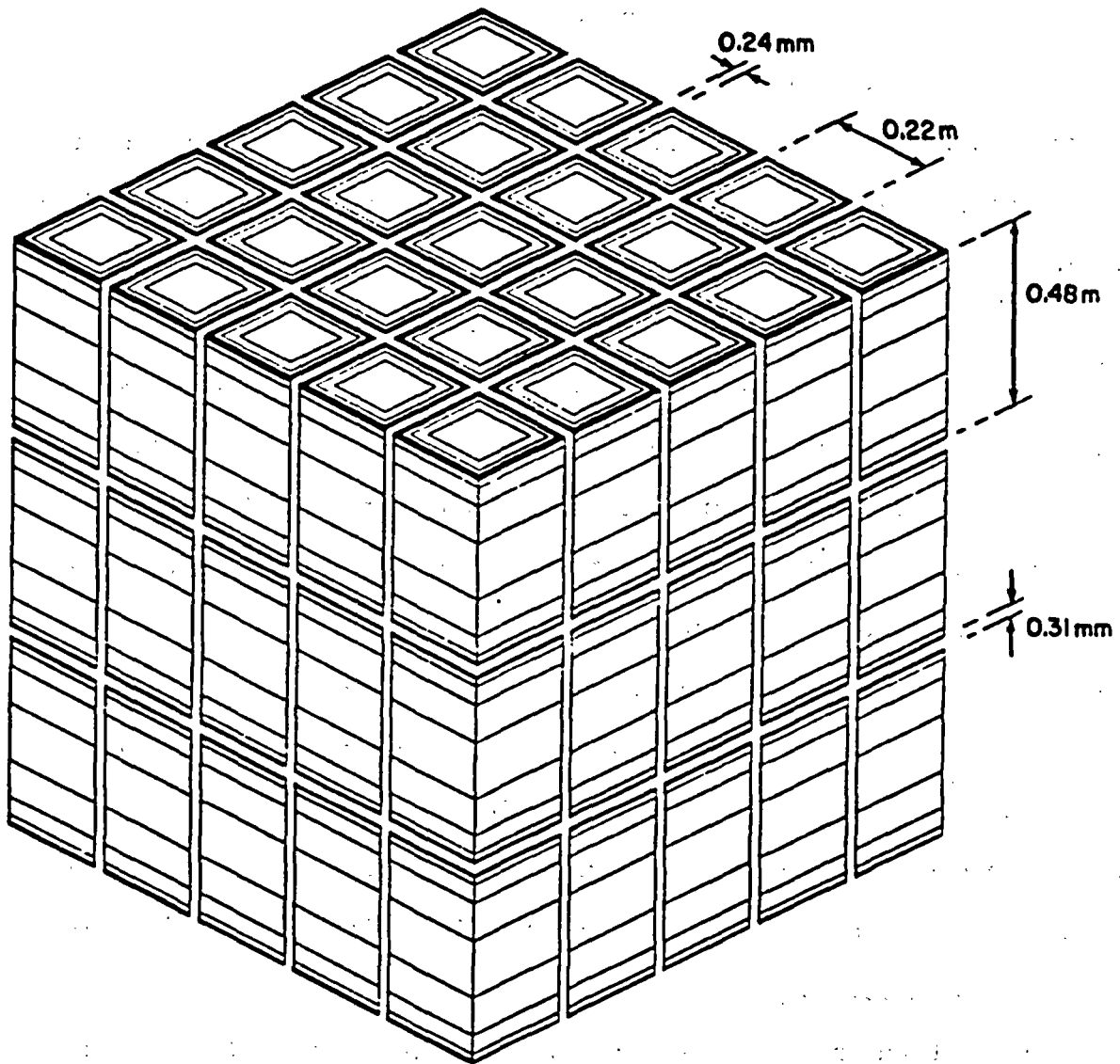
convenient to integrate numerically over the measured distribution and generate tabulated data for the effective fracture-matrix flow area.

With the use of extended memory, the modeling capabilities are increased to handle 2500 nodes and 5000 connections. All the arrays which depend on the nodal numbers and connection numbers are grouped together in the main program so that these arrays can be easily re-dimensionalized.

In addition to the efficient iterative solver, TRUST also can use the MA28 package for direct solution of the linear equations with a sparse variant of Gaussian elimination (Duff, 1977). All arrays for the MA28 routine are in large core memory. The direct solver is also used in the new version of the TRUST program to solve the steady fluid flow field.

FRACTURED TUFF COLUMN SIMULATIONS

A test case was set up to simulate the fluid flow in partially saturated, fractured, porous tuff. Simulations of vertical drainage within the Topopah Spring Member were performed. Two vertical fracture sets and one horizontal fracture set partitioned the tuff formation into blocks as shown in Figure 9. Figure 9 shows 5X5X3 blocks with each block's dimension being 0.2201 m x 0.2201 m x 0.4783 m. The fracture apertures, 0.2380 mm for the vertical fractures and 0.3082 mm for the horizontal fractures, are emphasized 100-fold in Figure 9. To simulate vertical drainage, only one vertical column bounded by four vertical fractures needs to be modeled. By symmetry, the midplanes of the bounding vertical fractures are no-flow boundaries. The horizontal fractures, normal to the direction of general flow, are explicitly simulated. On the local scale, lateral flow is allowed between



XBL842-9614

Figure 9. Discretization of fractured, porous tuff to represent densely welded Topopah Spring Member.

the vertical fractures and the matrix blocks. The horizontal cross section of the column is further partitioned into 6 nested elements and the vertical cross section of each block is sliced into 9 sections (Figure 10). The partition of horizontal nested elements is similar to that used in the MINC program (Pruess and Narasimhan, 1982) without grouping the matrix elements from different blocks together. The grid elements are small near the fractures and large toward the middle of the matrix block as shown in Figure 10 and tabulated in Table 1. 203 elements and 370 connections are used in the grid.

The conductances at the interfaces are determined by the harmonic means of the permeability values of the neighboring nodes weighted by the distances from the node centers to the interfaces. For the connections between the fracture and matrix, the distances from the fracture nodes to the interfaces are set to zero so that normal flow from matrix blocks to fractures is controlled by matrix permeability. The available area for flow across the fracture-matrix interfaces is determined by fracture saturations. At the limit that the fractures are completely desaturated, the available area is the contact area between adjacent blocks for matrix flow from one block to the next. The outermost matrix node for one block is connected to the fracture and is not directly connected to the matrix node in the next block in the simulations.

The upper boundary is a no-flow boundary. The lower boundary is a constant suction boundary. The suction head is maintained at -111.6 m, the in situ suction. Initially the system is fully saturated with pressure determined by hydrostatic equilibrium. The potential everywhere is zero and fluid is stationary. At $t = 0^+$, the negative suction head at the lower boundary begins to induce transient changes in the fluid flow field

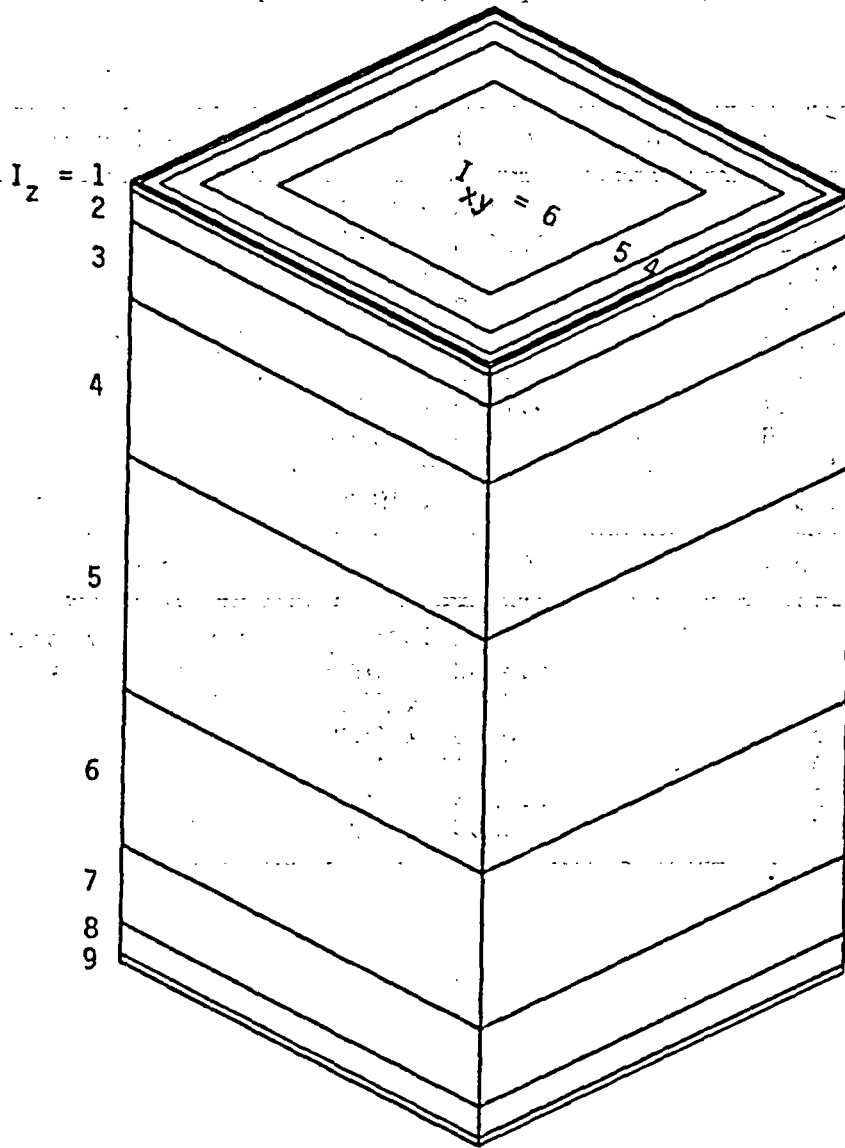


Figure 10. Discretization of one matrix block.

Table 1. Spacings of grid used in partially saturated, fractured, porous tuff simulations

Node Index I_z	$\Delta z(m)$	Material
1,11,21	4.6325×10^{-3}	Tuff Matrix
2,12,22	1.9146×10^{-2}	"
3,13,23	4.7866×10^{-2}	"
4,14,24	9.5732×10^{-2}	"
5,15,25	1.4360×10^{-1}	"
6,16,26	9.5732×10^{-2}	"
7,17,27	4.7866×10^{-2}	"
8,18,28	1.9146×10^{-2}	"
9,19,29	4.6325×10^{-3}	"
10,20	3.8024×10^{-4}	Horizontal Fracture

Node Index I_{xy}	$\Delta xy(m)$	Material
0	1.19×10^{-4}	Vertical Fracture
1	4.3362×10^{-4}	Tuff Matrix
2	2.2394×10^{-3}	"
3	5.8140×10^{-3}	"
4	1.27614×10^{-2}	"
5	2.3666×10^{-2}	"
6	1.3033×10^{-1}	"

throughout the fractured, porous tuff column. The TRUST program automatically controls the time steppings and iterations of nonlinear fracture and matrix properties. For the full simulations of the fractured-matrix drainage over a time span of 10^5 years the program requires 42 CPU sec on Lawrence Berkeley Laboratory's CDC7600 computer.

Five cases of flow in fractured, porous tuff were studied: (1) a fractured, porous column with the phase-separation constriction factor taken into account ($0 \leq \tau(h) \leq 1$) (2) a fractured, porous column without phase-separation constriction factor ($\tau = 1$), (3) a matrix column without fractures, (4) a discrete fracture network without matrix and with τ factor and (5) a discrete fracture network without matrix and without τ factor. The results are presented in plots of pressure head, saturation, permeability, effective fracture-matrix flow area, and Darcy velocity versus time at different locations (Figures 11-16). The locations of interests are the middle of the matrix block (point A), the middle of the vertical fracture (point B), the middle of the upper horizontal fracture (point C) and the middle of the lower horizontal fracture (point D) as shown in the inserts of the plots. We also plotted the velocities at the matrix-fracture interfaces at these mid-points and along the fractures at the fracture intersections.

Pressure Drop

Figure 11 shows the pressure drop at different locations in response to the negative suction at the lower boundary. The pressure heads decrease from the initial positive hydrostatic pressure and become negative at 10^{-5} years for Case 1 and the pressure heads decrease more gradually at earlier times for Case 2. After the pressure drop at 10^{-5} years for Case 1, a small

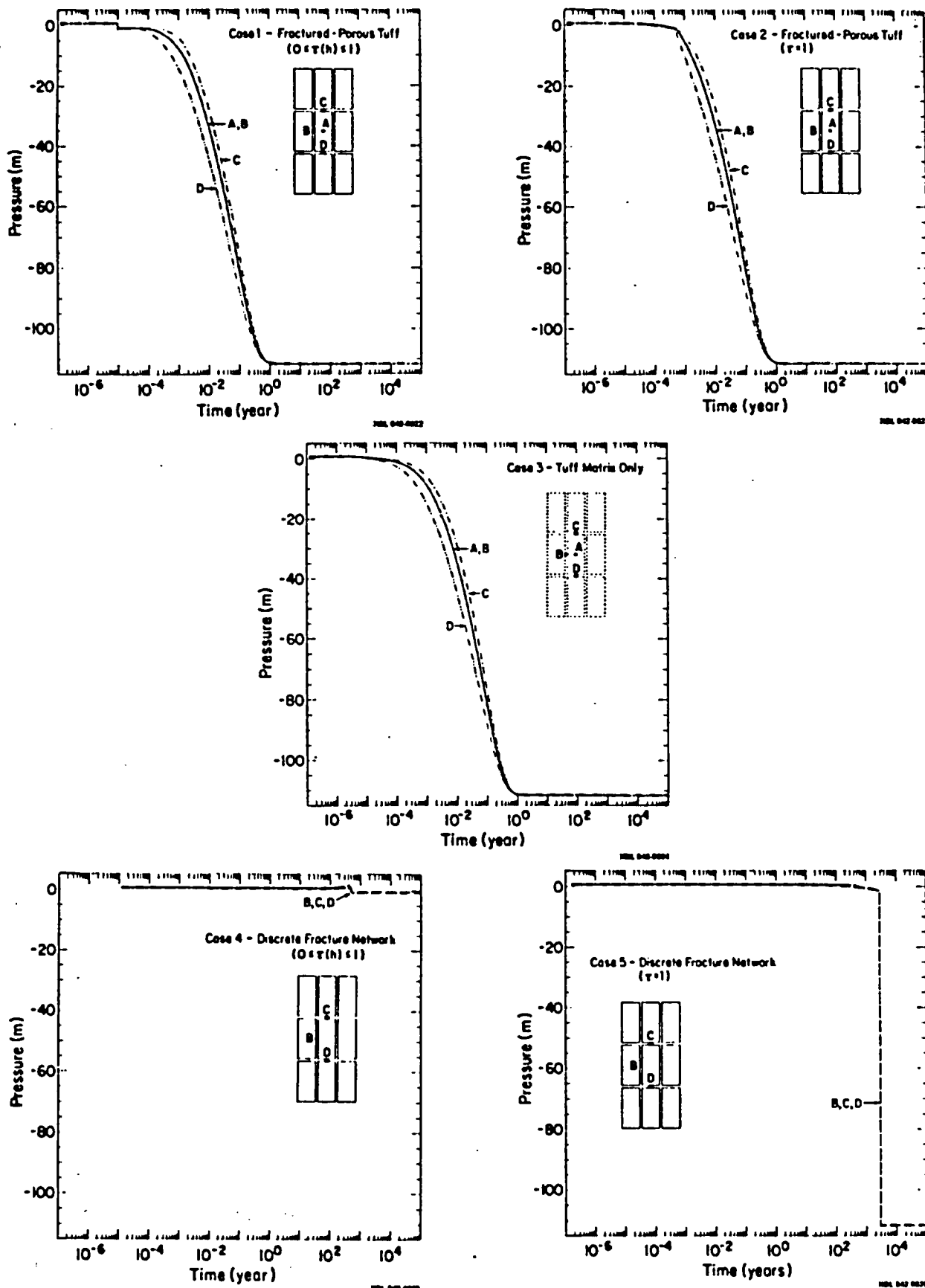


Figure 11. Pressure drops.

but noticeable increase in pressure is observed in the simulated results before large decreases at later times.

As pressures become negative following initial desaturations, the pressure changes are controlled mainly by the matrix. Cases 1, 2, and 3 are essentially the same after 10^{-2} years. The lower fracture, Point D, is closer to the suction boundary and has more negative pressure than the higher elevation points. At the same elevation, the matrix pressure at Point A and the vertical fracture pressure at Point B are approximately the same. Therefore, pressure changes can be simulated with matrix properties only, if the transition from saturated conditions to unsaturated conditions is not of interest.

Very different results are obtained if the changes in a fractured-porous system are simulated only through the discrete fracture network (Cases 4 and 5 in Figure 11). Taking into account the phase-separation constriction effects (Case 4), the fractures remain at pressures near zero during the entire simulation period of 10^5 years. If the phase-separation constriction factor is not taken into account (Case 5), the fractures will respond to the negative suction, but at extremely long times as a result of the highly nonlinear fracture characteristic curves. Without the presence of matrix blocks to act as flow channels for fluid to change pressures, unrealistic results are obtained.

Saturation Change

Figure 12 illustrates the saturation changes at different points for the five cases. In Cases 1 and 2 for the fractured, porous tuff column, the fracture saturation drops abruptly at early times. The matrix changes more slowly from the initial fully saturated condition of $S = 1$ to the final ambient saturation of $S = 0.8$. The desaturation of fractures are

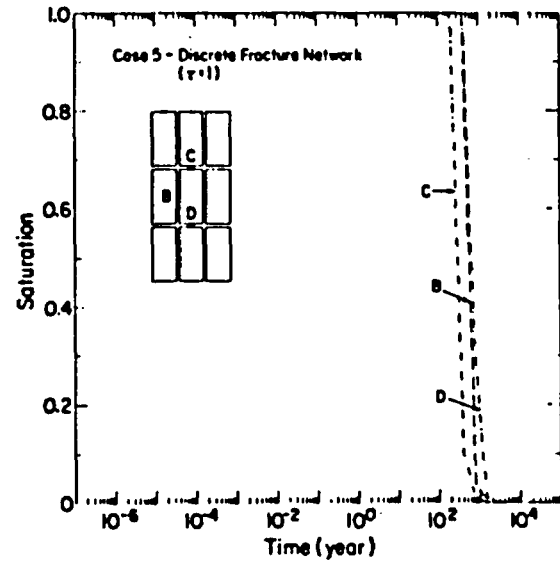
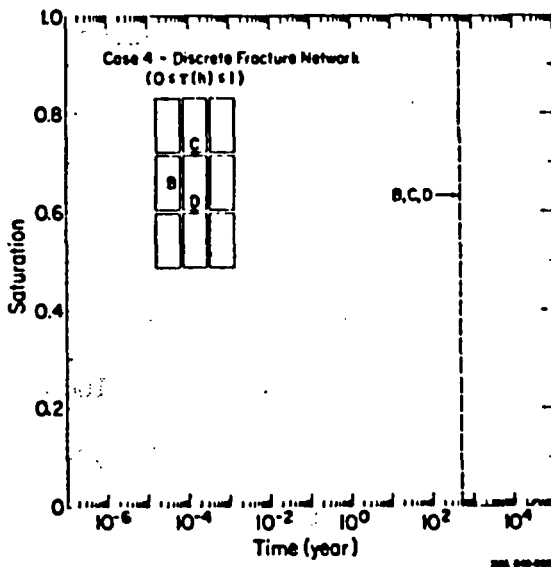
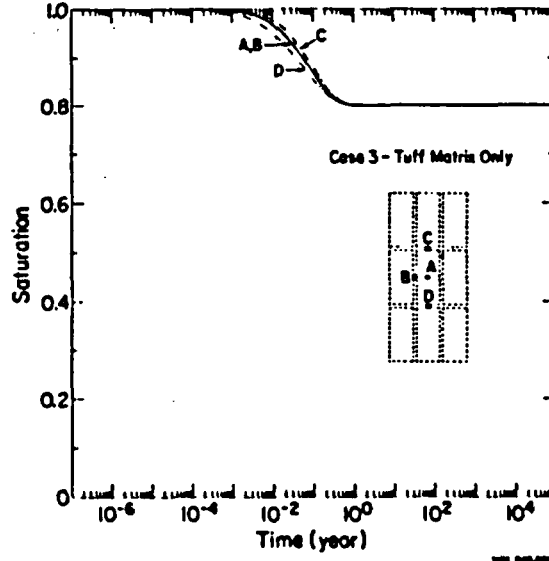
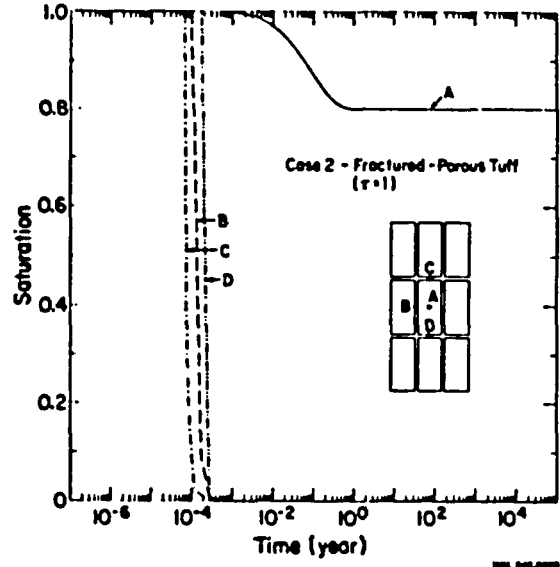
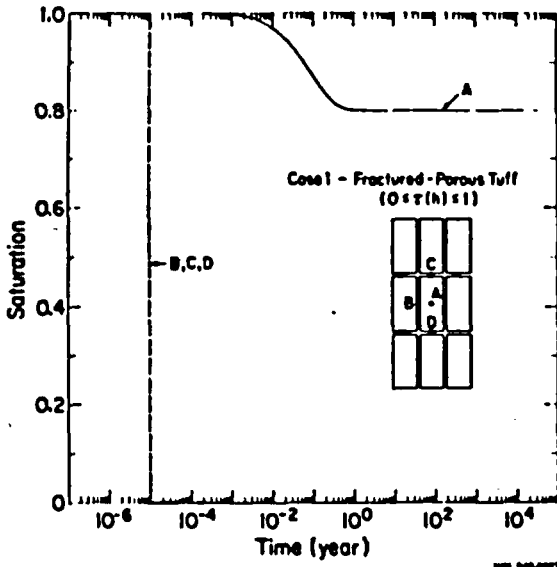


Figure 12. Saturation changes.

sensitive to the phase-separation constriction factor. In Case 1 and Case 4 with $0 \leq \tau(h) \leq 1$, the saturation changes at different fracture locations occur essentially at the same time while for Case 2 and Case 5 with $\tau = 1$, the upper horizontal fracture (Point C) desaturates first, followed by desaturation at vertical fracture (Point B) of middle elevation and the lower horizontal fracture (Point C) desaturates last. Case 4 in Figure 12 shows that fracture saturation does drop from $S = 1$ to nearly $S = 0$ with the small pressure changes illustrated in Case 4 of Figure 11.

The rates of the simulated saturation changes shed light on the feasibility of laboratory studies of fractured-tuff properties. For the 1.44 m long tuff column simulated in this analysis, a change in matrix saturation of $\Delta S = 0.2$ requires 10^{-2} to 1 year for the matrix to respond to the suction on the lower boundary. If the experiments were carried out over shorter time spans, the observation of saturation changes would be unreliable. On the other hand, saturation changes in the fractures will occur very abruptly. Therefore, instruments to detect saturation changes must have high resolution to detect the desaturation processes.

Permeability Change

Figure 13 shows the permeability changes at different points for the five cases. The permeability changes illustrate even more drastically than the saturation changes the contrast in behavior between fractures and porous matrix. Case 1 indicates that fractures will stop transmitting fluid 10^{-5} years after the suction begins as the fracture permeability vanishes. The matrix permeability changes by less than an order of magnitude from the initial condition of $S = 1$ to the final condition of $S = 0.8$. Initially the

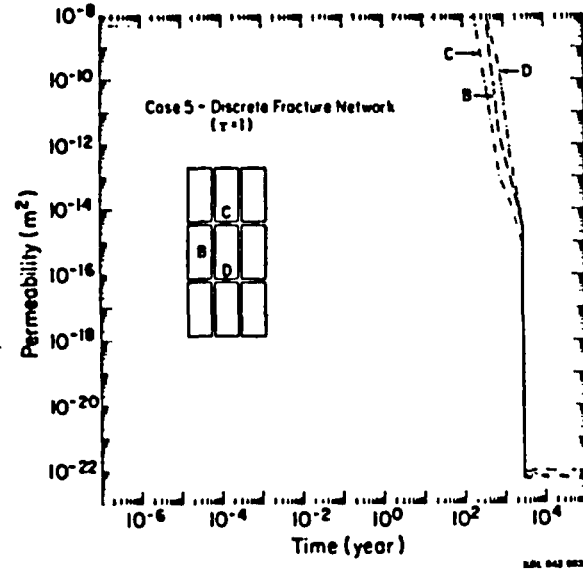
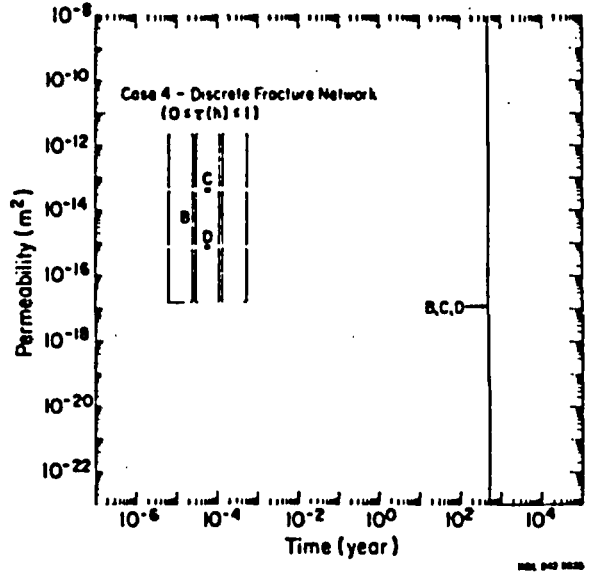
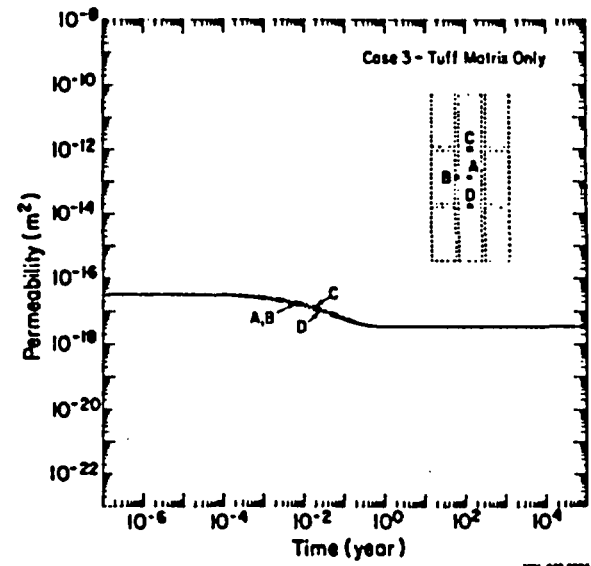
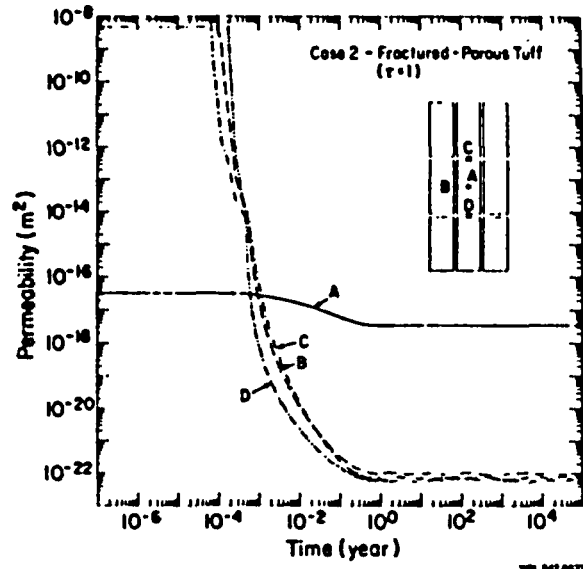
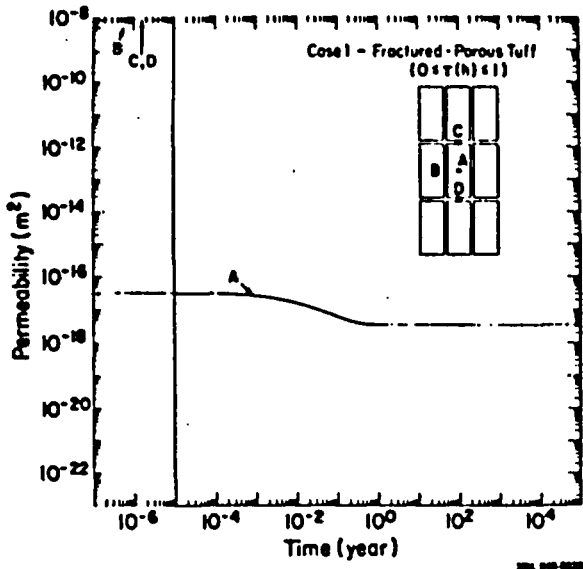


Figure 13. Permeability changes.

fracture permeabilities of each discrete fracture are more than 8 orders of magnitude greater than the matrix permeability. The fracture permeability changes are sensitive to the phase-separation constriction factor as shown in the difference between Case 1 with $0 \leq \tau(h) \leq 1$ and Case 2 with $\tau = 1$. For Case 2, the fractures will remain conductive at the final ambient conditions with the permeabilities more than 4 orders of magnitude smaller than the matrix permeability. However, Case 2 with $\tau = 1$ does not account for the possibility that the liquid phase may become discontinuous, thereby blocking flow.

Effective Fracture - Matrix Flow Area Change

Figure 14 illustrates the changes in the effective area at the midpoints of fractures for flow across the matrix-fracture interfaces for Case 1 and Case 2. As the fractures desaturate, the wetted area on the fracture surfaces decreases. At complete desaturation, only the contact area, which is $\omega = 12\%$ of fracture surface in these simulations, is available for fluid flow from one matrix across fractures to the next matrix block. This reduction in effective fracture-matrix flow area may significantly change the actual flow paths for fluid movement.

Darcy Velocity Changes in Fractures

Figure 15 illustrates the changes in Darcy velocities at the fracture intersections for Case 1 and Case 2. Before the fractures desaturate, fluid mainly flows downward along the vertical fractures. The downward velocity increases rapidly and peaks just before the fractures desaturate. After the transition to matrix flow, fluid velocities in fractures are essentially zero. The flows in the fracture at different locations are sensitive to the phase-separation constriction factor. In Case 2 with $\tau = 1$,

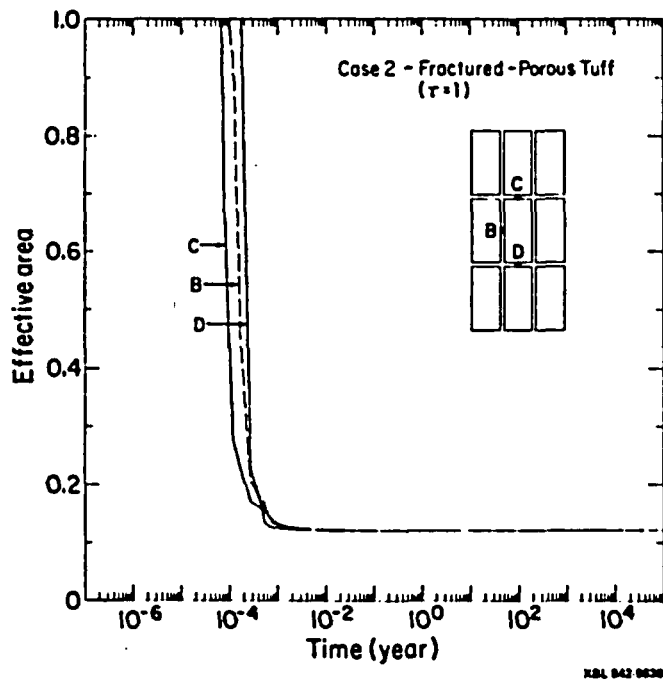
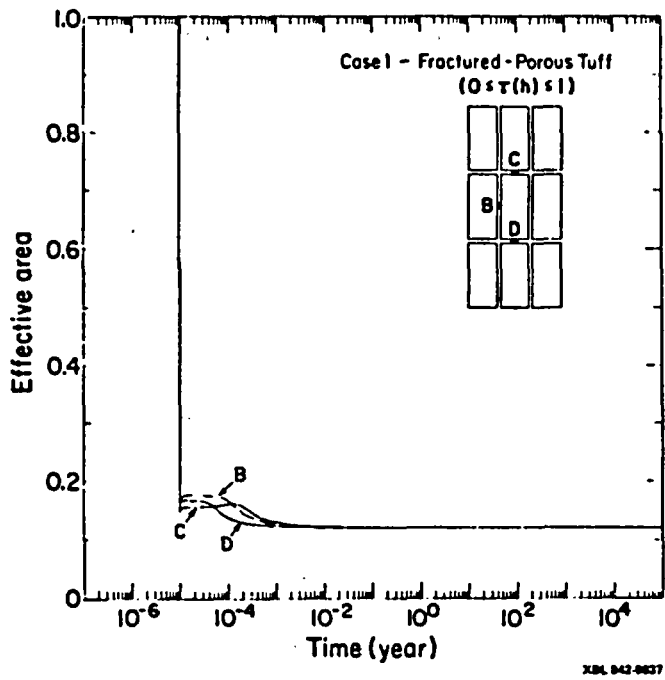


Figure 14. Effective fracture-matrix flow area changes.

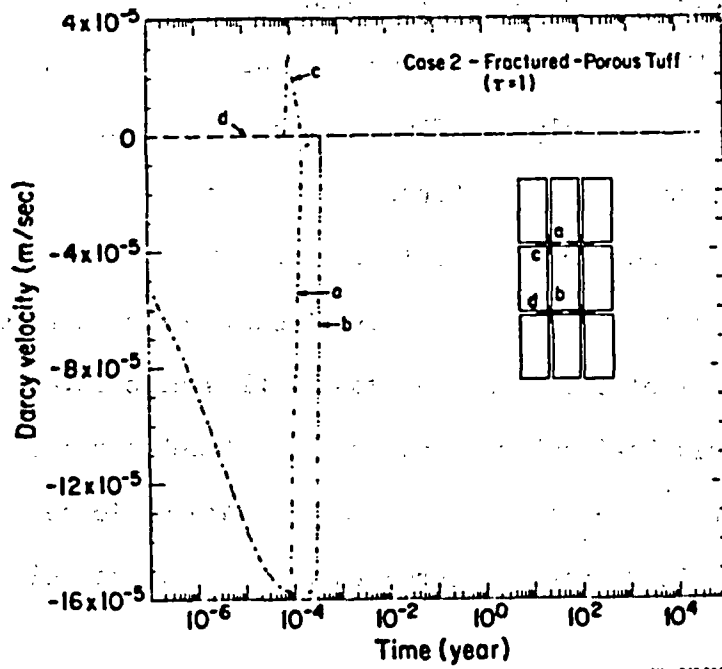
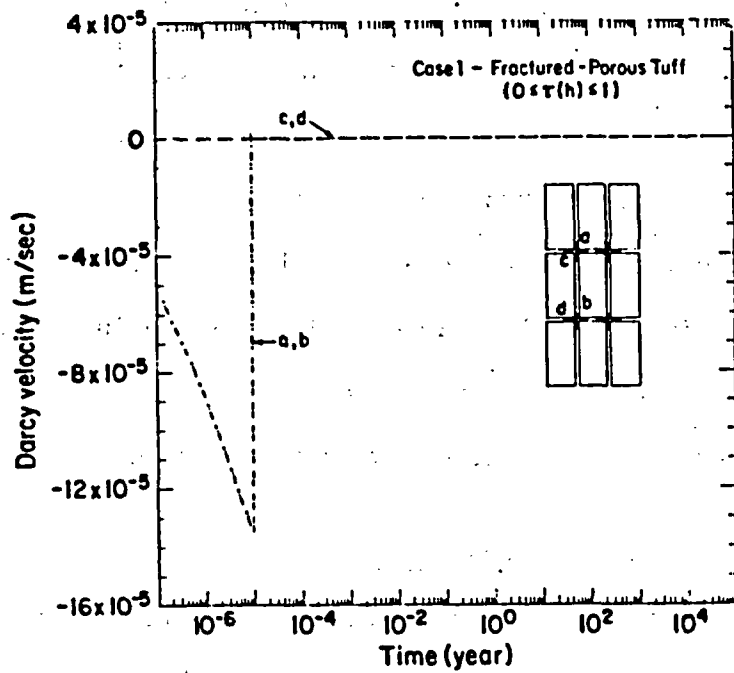


Figure 15. Darcy velocities along discrete fractures (sign convention for horizontal flow: positive - into the intersection, negative - away from the intersection; vertical flow: positive - upward, negative - downward).

the fluid moves more easily through the fractures before desaturation than in Case 1 with $0 \leq \tau(h) \leq 1$. The differences in velocities at different locations for Case 2 are more pronounced than for Case 1. The fluid in horizontal fractures moves towards the vertical fractures before they are drained. Just before vertical fracture flow stops, horizontal flow peaks. This is more evident in Case 2 than in Case 1. This again indicates that fracture flow in the transition from saturated to desaturated condition is sensitive to the details of fracture-flow characteristics.

Darcy Velocity Changes in Fracture-Matrix Interfaces

Figure 16 illustrates the changes in Darcy velocities across the fracture-matrix interfaces at the mid-points of fractures. The fracture-matrix flow velocities are much smaller than the fracture flow velocities in Figure 15. Before the fractures desaturate, the fluid in the matrix flows toward the fractures to supply the fluid in the fractures which is drained rapidly by the suction. At the saturated-desaturated transition, these matrix-fracture flows change drastically. After the transition, the fluid mainly moves vertically from upper matrix blocks, across horizontal fractures, and into lower matrix blocks. The horizontal flow also reverses direction from an initial matrix-to-fracture flow to a small but significant fracture-to-matrix flow. After the transition, the fracture no longer transmits fluid and becomes a small fluid storage source to feed the matrix blocks as they drain.

After the fractures desaturate, the Darcy velocities from one matrix block across the fracture into the next matrix block are essentially the same as those calculated by a matrix-only model, as illustrated in Case 3, Figure 16 for a tuff matrix column without fractures. The agreement among

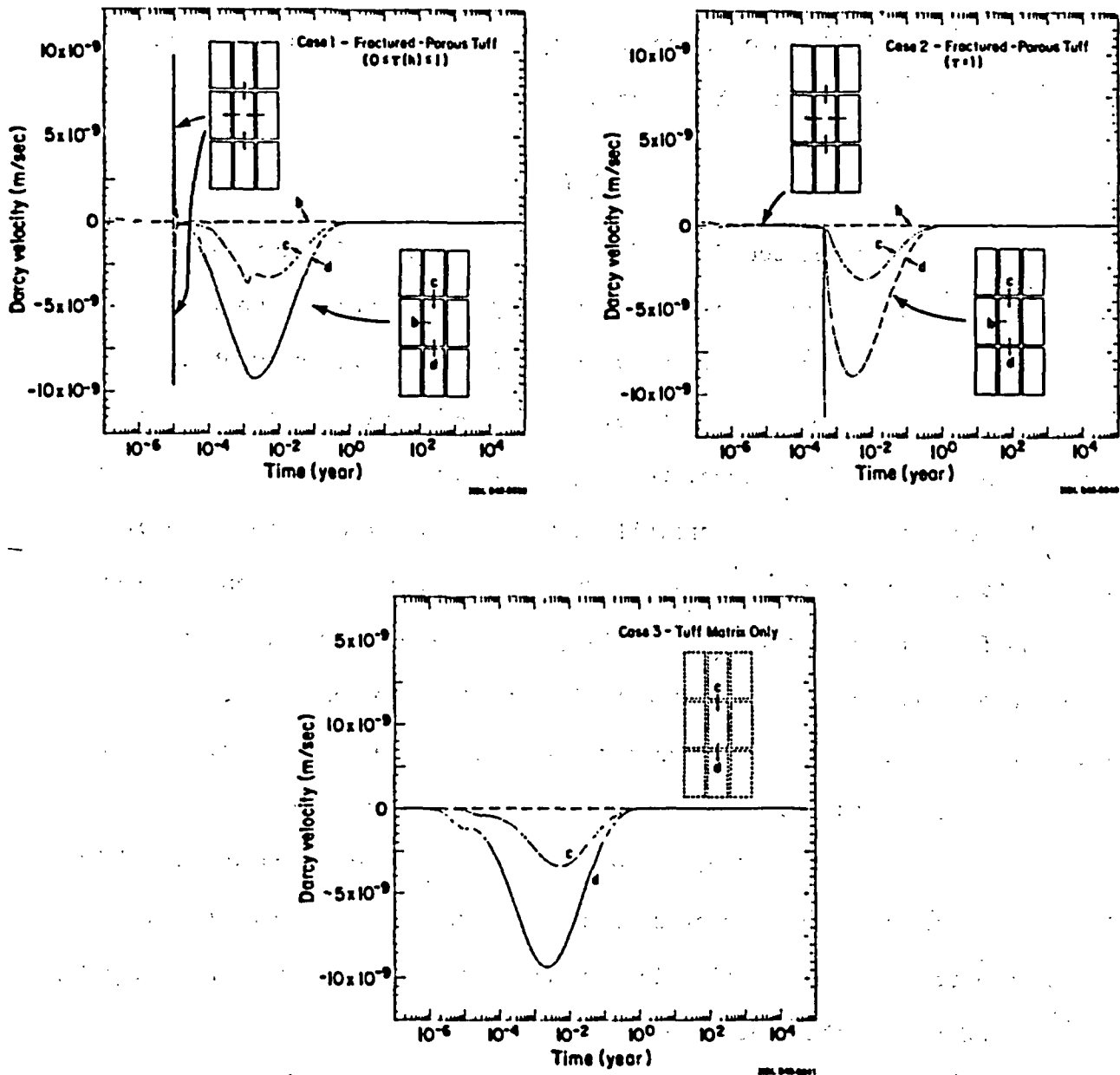


Figure 16. Darcy velocities at the fracture-matrix interfaces (sign convention for horizontal flow: positive - matrix into fracture, negative - fracture into matrix; vertical flow: positive - upward, negative - downward).

the velocities in Cases 1, 2, and 3 strongly indicate that the fluid flow field of a partially saturated fractured, porous formation can be simulated without taking fractures into account, if the transition region from saturated to unsaturated condition is not of concern.

SUMMARY

From the cases simulated for a fractured, porous tuff column with discrete fractures and porous blocks explicitly taken into account, the quasi-steady changes of the fluid flow field of a partially saturated, fractured, porous system could be simulated approximately without taking fractures into account. However, the highly transient changes in flow from fully saturated conditions to partially saturated conditions are extremely sensitive to the fracture properties. On the one hand, the ambient, steady-state flow field of a partially saturated, fractured porous tuff system probably can be understood without detailed knowledge of the discrete fracture network properties. Under large suctions, the porous matrix is the main conduit for fluid flow. On the other hand, detailed information on fracture network geometry and discrete fracture characteristics is needed to fully understand the responses of a fractured-porous system to perturbations such as an extreme flood event, which may cause transitions between partially saturated and fully saturated conditions.

Only one set of material properties has been simulated for the Topopah Spring Member. Not all of the required properties for simulations of the fractured tuff are available. We have developed a statistical theory and have derived explicit formulae for the fracture characteristics based on well established capillarity theory and recent advances in rough fracture flow laws. The input data for the fracture properties, such as the spacing

and the aperture distribution parameters are derived from available fracture data. Some of the simplistic assumptions about fracture properties can be easily modified as more data become available. We expect that we will gain additional physical insight as we study more realistic simulations.

We believe that our basic conceptual model, based on an extension of soil physics of heterogeneous systems to a fractured, porous medium, is sound. Some of the detailed descriptions and assumptions, such as the reduction of the effective fracture-matrix flow area and the existence of a discontinuous liquid phase on the fracture surfaces, should become better established as experimental verification and more detailed numerical simulations are obtained. The tools needed for detailed numerical simulations are available. The logical task now is to closely couple these capabilities and modeling exercises with experimental investigations to better understand and assess the impact of a repository on the hydrology of the partially saturated fractured, porous tuff formations.

REFERENCES

- Blair, S. C., P. R. Heller, G. W. Gee, I. J. Hall, and R. R. Peters, 1984. Fracture and matrix permeability and water retention characteristics of tuffaceous materials from the Nevada Test Site, Report SAND 83-7474, 49 p., Sandia National Laboratories, Albuquerque, NM.
- Boussinesq, J., 1868. Memoire sur l'influence des frottements dans les mouvements repuliers des fluides, J. Math. Pure Appl. Ser. 2, Vol. 13, pp. 377-424.
- Carr, W. J. , 1974. Summary of tectonic and structural evidence for stress orientation at the Nevada Test Site, U.S. Geological Survey Report OFR-74-176, 53 p.
- Duff, I. S., 1977. MA28 - A set of Fortran subroutines for sparse unsymmetric linear equations, Report AERE-R 8730, Harwell/Oxfordshire, Great Britain.
- Evans, D. D. and C. H. Huang, 1982. Role of desaturation on transport through fractured rock, in "Role of the Unsaturated Zone in Radioactive and Hazardous Waste Disposal", pp. 165-178, edited by J. Mercer, P. S. Rao and I. W. Marine, Ann Arbor Science Publisher, Ann Arbor, MI.
- Hayden, H., R. R. Peters and J. K. Johnstone, 1983. Parameters and material properties for hydrologic modeling of the Topopah Spring Unit, memorandum to distribution, 9/27/83, Sandia National Laboratories, Albuquerque, NM.
- Iwai, K., 1976. Fundamental Studies of Fluid Flow Through a Single Fracture, Ph.D. Thesis, Department of Civil Engineering, University of California, Berkeley, CA., 208 p.
- Mualem, Y. 1976. A new model for predicting the hydrologic conductivity of unsaturated porous media, Water Resources Research, Vol. 12, pp. 513-522.
- Narasimhan, T. N., P.A. Witherspoon and A. L. Edwards, 1978. Numerical model for saturated-unsaturated flow in deformable porous media, Part 2, the algorithm, Water Resources Research, Vol 14, pp. 255-261.
- Pickens, J. F., R. W. Gillham and D. R. Cameron, 1979. Finite-element analysis of the transport of water as solute in tile-drained soils, J. Hydrology, Vol. 4, pp. 243-264.
- Peters, R. R., and J. H. Gauthier, 1984. Results of TOSPACE hydrologic calculation for Yucca Mountain, memorandum to F. W. Bingham, 4/30/84, 12 p., Sandia National Laboratories, Albuquerque, NM.
- Pruess, K. and T. N. Narasimhan, 1982. A practical method for modeling fluid and heat flow in fractured porous media, Paper SPE-10509, Proceedings of the Society of Petroleum Engineering Symposium on Reservoir Simulation, New Orleans, LA., pp. 269-284.

REFERENCES

- Scott, R. B., R. W. Spengler, S. Diehl, A. R. Lappin, and M. P. Chornack, 1982. Geologic character of tuffs in the unsaturated zone at Yucca Mountain, Southern Nevada, in "Role of the Unsaturated Zone in Radioactive and Hazardous Waste Disposal", pp. 289-335, edited by J. Mercer, P. S. Rao and I. W. Marine, Ann Arbor Science Publisher, Ann Arbor, MI.
- Sinnock, S., Y. T. Lin, and J. P. Brannen, 1984. Preliminary bounds on the expected, postclosure performance of the Yucca Mountain repository site, Southern Nevada, Report SAND 84-1492, Sandia National Laboratories, Albuquerque, NM.
- Spengler, R. W. and M. P. Chornack, 1984. Stratigraphic and structural characteristics of volcanic rocks in core hole USW-G4, Yucca Mountain, Nye County, Nevada, with a section of geophysical logs by D. C. Muller and J. E. Kibler, Report USGS-DFR-84- , U. S. Geological Survey, Denver, CO.
- Thordarson, W., 1983. Geohydrologic data and test results from well J-13, Nevada Test Site, Nye County, Nevada, Report Water Resources Investigations 83-4171, U.S. Geological Survey, Denver, CO.
- Tsang, Y. W. and P. A. Witherspoon, 1981. Hydromechanical behavior of a deformable rock fracture, J. Geophysical Research, Vol. 86 (B10), pp. 9287-9298.
- Tsang, Y. W., 1984. The effect of tortuosity on fluid flow through a single fracture, Water Resources Research, to be published.
- Tyler, L. D., 1983. Minutes of June 23-24 Performance Assessment Working Group Meeting, memorandum to distribution, 7/29/83, Sandia National Laboratories, Albuquerque, NM.
- van Genuchten, 1980. A closed-form equation for predicting the hydraulic conductivity of unsaturated soils, Soil Sci. Soc. Am. J., Vol. 44, pp. 892-898.
- Winograd, I. J. and W. Thordarson, 1975. Hydrogeologic and hydrochemical framework, South Central Great Basin, Nevada-California, with Special Reference to the Nevada Test Site, U. S. Geological Survey Professional Paper 712-C, pp. C1-126.
- Witherspoon, P. A., J. S. Y. Wang, K. Iwai, and J. E. Gale, 1980, Validity of cubic law for fluid flow in a deformable rock fracture, Water Resources Research, Vol. 16, pp. 1016-1024.

This report was done with support from the Department of Energy. Any conclusions or opinions expressed in this report represent solely those of the author(s) and not necessarily those of The Regents of the University of California, the Lawrence Berkeley Laboratory or the Department of Energy.

Reference to a company or product name does not imply approval or recommendation of the product by the University of California or the U.S. Department of Energy to the exclusion of others that may be suitable.

TECHNICAL INFORMATION DEPARTMENT
LAWRENCE BERKELEY LABORATORY
UNIVERSITY OF CALIFORNIA
BERKELEY, CALIFORNIA 94720